JOURNAL OF GEOPHYSICAL RESEARCH, VOL. 111, C06032, doi:10.1029/2005JC003282, 2006

Spatial patterns in seasonal and interannual variability of chlorophyll and sea surface temperature in the California Current

Kasey R. Legaard[1] and Andrew C. Thomas[1]

Received 6 September 2005; revised 10 February 2006; accepted 13 March 2006; published 24 June 2006.

[1] Physical forcing and biological response within the California Current System (CCS) are highly variable over a wide range of scales. Satellite remote sensing offers the only feasible means of quantifying this variability over the full extent of the CCS. Using six years (1997–2003) of daily SST and chlorophyll imagery, we map the spatial dependence of dominant temporal variability at resolutions sufficient to identify recurrent mesoscale circulation and local pattern associated with coastal topography. Here we describe mean seasonal cycles and interannual variation; intraseasonal variability is left to a companion paper (K. R. Legaard and A. C. Thomas, manuscript in preparation, 2006). Coastal upwelling dictates seasonality along north-central California, where weak cycles of SST fluctuate between spring minima and late summer maxima and chlorophyll peaks in early summer. Off northern California, chlorophyll maxima are bounded offshore by the seasonally recurrent upwelling jet. Seasonal cycles differ across higher latitudes and in the midlatitude Southern California Bight, where upwelling winds are less vigorous and/or persistent. Seasonality along south-central Baja is strongly affected by processes other than upwelling, despite year-round upwelling-favorable winds. Interannual variation is generally dominated by El Niño and La Niña conditions. Interannual SST variance is greatest along south-central Baja, although interannual variability constitutes a greater fraction of total variance inshore along southern Oregon and much of California. Patterns of interannual chlorophyll variance are consistent with dominant forcing through the widespread depression and elevation of the nutricline during El Niño and La Niña, respectively. Interannual variability constitutes a greater fraction of total chlorophyll variance offshore.

Citation: Legaard, K. R., and A. C. Thomas (2006), Spatial patterns in seasonal and interannual variability of chlorophyll and sea surface temperature in the California Current, *J. Geophys. Res.*, *111*, C06032, doi:10.1029/2005JC003282.

1. Introduction

[2] The California Current System (CCS) extends along the west coast of North America from Vancouver Island to the tip of Baja California. Typical of major eastern boundary current systems, coastal upwelling driven by persistent equatorward wind fuels heightened primary production and elevated phytoplankton biomass. Physical and biological processes within the CCS vary over a wide range of time and space scales [see *Hutchings et al.*, 1995; *Smith*, 1995; *Hickey*, 1998; *Hill et al.*, 1998; *Mackas et al.*, 2006]. Large-scale wind systems force latitudinally dependent seasonal cycles of oceanic processes, including the seasonally recurrent formation of an energetic system of mesoscale jets and eddies. Coastal topography and shelf/slope morphology impose local variation. Wind forcing is pulsed over periods of days to weeks, even at locations of sustained upwelling. Scales of physical variability closely match those of the life cycles of dominant plankton, leading to strong interactions between physical and biological processes [*Denman and Powell*, 1984]. Basin-scale oceanic and atmospheric processes modify patterns of physical forcing and biological response over interannual and decadal scales.

[3] Multiyear time series of satellite-derived sea surface temperature (SST) and surface chlorophyll concentrations provide the sole means by which concurrent patterns of physical and biological variability can be synoptically viewed and systematically quantified across the entire California Current region. Descriptions of seasonal variations based on multiyear time series of satellite imagery have typically focused on temporally binned data (image composites) and/or specific locales over which spatial variations are apparent but data are averaged [e.g., *Michaelsen et al.*, 1988; *Strub et al.*, 1990; *Thomas and Strub*, 1990; *Thomas et al.*, 1994, 2001, 2003; *Kahru and Mitchell*, 2001; *Sackmann et al.*, 2004]. Quantitative analyses of intraseasonal or mesoscale SST or chlorophyll variability within the CCS have typically been limited to narrow spatial or temporal windows defined by relatively cloud-free imagery [e.g., *Kelly*, 1985; *Denman and Abbott*, 1988, 1994; *Smith et al.*, 1988; *Abbott and Barksdale*, 1991; *Gallaudet and Simpson*, 1994; *Armstrong*, 2000].

[1]School of Marine Sciences, University of Maine, Orono, Maine, USA.

0148-0227/06/2005JC003282$09.00

[4] Our goal is to quantify and compare physical and biological variability across the CCS (Figure 1), mapping the spatial dependence of dominant patterns of temporal variability at resolutions sufficient to identify the role of recurrent mesoscale circulation and local processes associated with coastal topography. We quantify patterns of variability acting over seasonal, interannual, and intraseasonal timescales from nearly six years (1997–2003) of daily SST and chlorophyll data. Here we describe and discuss patterns of seasonal and interannual variability. Patterns of intraseasonal variability are left to a companion paper (K. R. Legaard and A. C. Thomas, manuscript in preparation, 2006). Section 2 provides a brief description of relevant processes forcing near-surface variability within the CCS, and a brief description of prior satellite-based research. Data and methods are described in section 3. Results and discussion of seasonal and interannual variability are merged into section 4. Section 5 is a brief summary.

2. Background

[5] Upwelling winds throughout the CCS are driven by anticyclonic circulation around the North Pacific subtropical high-pressure system. The North Pacific high attains its most northerly position and greatest strength in late spring and summer, coincident with the strengthening and expansion of a thermal low over the southwest U.S. and Mexico [*Nelson and Husby*, 1983; *Strub and James*, 1988]. Coastal winds driven by the pressure gradient between these two systems are generally equatorward and upwelling-favorable along the entire coastline [*Halliwell and Allen*, 1987; *Dorman and Winant*, 1995]. Propagating storms are diverted to the north where they force more variable winds across the Pacific Northwest [*Dorman and Winant*, 1995]. Equatorward winds are channeled along the coastal mountains of northern and central California, forcing strong and sustained upwelling often localized within upwelling centers downwind of major headlands [*Beardsley et al.*, 1987; *Dorman and Winant*, 1995; *Edwards et al.*, 2002]. During mid to late fall, high pressure weakens and retreats to the south ahead of an expanding and deepening Aleutian low [*Strub and James*, 1988]. Monthly mean wind stress is poleward and downwelling-favorable along northern California and the Pacific Northwest. Upwelling-favorable winds persist with diminished strength along central California and the Baja Peninsula [*Halliwell and Allen*, 1987; *Dorman and Winant*, 1995]. South of Point Conception (34.4°N), the Southern California Bight (SCB) (Figure 1) forms an area sheltered year-round from the stronger wind-forcing to the north and south [*Dorman and Winant*, 1995; *Winant and Dorman*, 1997].

[6] The spring transition to strong and persistent equatorward winds is accompanied by an abrupt transition in nearshore currents and water properties. Coastal sea levels drop as relatively cold, saline water is upwelled over the shelf and upper slope [*Strub et al.*, 1987; *Strub and James*, 1988] leading to the formation of a coastal upwelling front and a narrow, surface-intensified geostrophic jet [*Smith*, 1995]. Formation of the coastal jet reverses inshore poleward flow along the U.S. coast and either reverses poleward flow or reinforces equatorward flow along the Baja coast [*Lynn and Simpson*, 1987; *Strub et al.*, 1987; *Strub and James*, 2000]. The upwelling jet remains over the shelf and slope of the Pacific Northwest but is quickly displaced seaward south of Cape Blanco, Oregon (42.8°N) (Figure 1) as the high-velocity core of the California Current [*Barth et al.*, 2000; *Strub and James*, 2000; *Lynn et al.*, 2003]. Various instability processes produce meanders that develop into cyclonic and anticyclonic eddies to either side of the current core [*Marchesiello et al.*, 2003]. Cool and productive water flows seaward within narrow filaments lying along the inshore edges of the offshore-directed legs of prominent meanders. Vigorous jet and eddy activity promotes rapid exchange between shelf waters and the open ocean and provides a local source of enrichment to offshore waters through geostrophic adjustment [*Hood et al.*, 1990, 1991; *Chavez et al.*, 1991; *Strub et al.*, 1991]. By late summer, equatorward winds weaken, coastal sea levels rise, and an inshore poleward countercurrent develops along southern and central California and along parts of the Baja Peninsula [*Lynn and Simpson*, 1987; *Strub and James*, 2000]. Poleward coastal currents strengthen and extend northward, displacing the upwelling jet from the shelves of the Pacific Northwest. The entire jet and eddy system

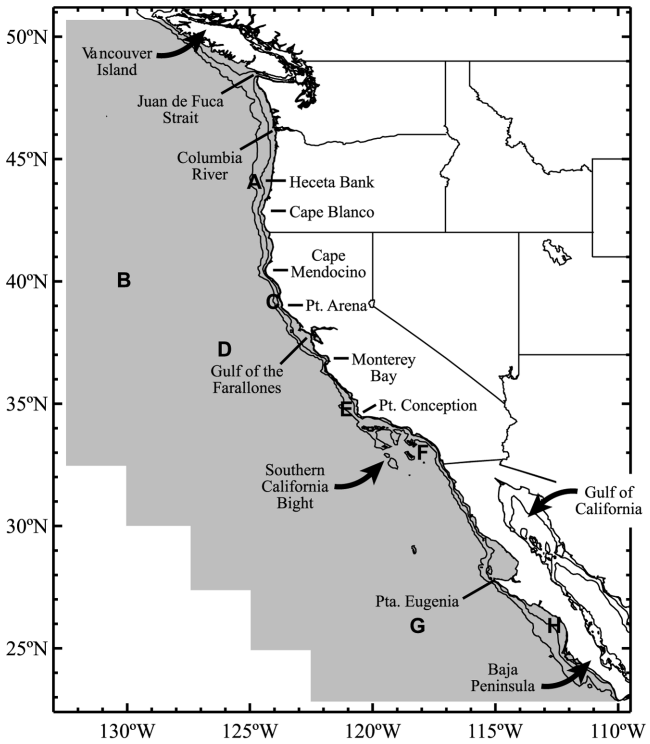

Figure 1. Map of the California Current study region, showing the area of interest (shaded) and the locations of time series data discussed within the text (A–G). Time series locations and their approximate water depths are as follows: A, Heceta Bank, 200 m; B, northern California offshore, >3000 m; C, Pt. Arena, 600 m; D, central California offshore, >3000 m; E, Pt. Conception, 300 m; F, eastern Southern California Bight, 600 m; G, southern Baja offshore, >3000 m; and H, southern Baja inshore, <100 m. Locations C and E coincide with NOAA NDBC stations 46014 and 46023, respectively. Also included are 100 and 500 m isobaths.

migrates westward and gradually decays through the fall and winter [*Strub and James*, 2000].

[7] The reiterative, synoptic views offered by satellite observations of SST and chlorophyll are well suited for characterizing dominant spatial and temporal patterns of near-surface physical and biological variability. Studies of mesoscale variation have generally focused on summer months. From a quantitative analysis of SST imagery collected off northern California, *Kelly* [1985] identify coherent patterns associated with local variations in wind-forcing superimposed over a large-scale seasonal warming trend. Multiyear time series of SST imagery collected off central California and the Baja Peninsula demonstrate seasonally recurrent mesoscale patterns in close association with coastal topography and/or spatial variations in wind forcing [*Lagerloef*, 1992; *Gallaudet and Simpson*, 1994; *Armstrong*, 2000]. Coastal Zone Color Scanner (CZCS) imagery of central California show rapid changes of phytoplankton pigment patterns following changes in wind forcing, superimposed over persistent and seasonally recurrent structure associated with upwelling filaments and eddies [*Abbott and Barksdale*, 1991]. Spectral statistics of pigment and SST imagery suggest that over timescales of days to several weeks, phytoplankton behave largely as passive tracers of mesoscale circulation, with growth, death, and sinking affecting near-surface pigment distributions only minimally [*Smith et al.*, 1988; *Denman and Abbott*, 1994].

[8] More than seven years of pigment data collected by CZCS (1978–1986) provide a general depiction of mean seasonality across the CCS [*Strub et al.*, 1990; *Abbott and Barksdale*, 1991; *Thomas et al.*, 1994; *Thomas and Strub*, 2001]. A typically diffuse and widespread bloom occurs at the onset of the upwelling season, after which pigment distributions collapse inshore to form a sharp frontal gradient coincident with the upwelling jet. A diffuse expansion of elevated concentrations typically follows in early fall. Offshore concentrations subsequently drop to low winter levels while elevated concentrations persist along a narrow coastal band. This generalized seasonal cycle is strongest off central California and weakest within the SCB and off northern Baja [*Thomas et al.*, 1994; *Thomas and Strub*, 2001]. Large-scale variations in pigment distributions are generally in phase and correlated with wind forcing, although the strength of this relationship varies greatly with latitude and between seasons [*Abbott and Barksdale*, 1991; *Thomas and Strub*, 2001]. Chlorophyll imagery collected by the Sea-viewing Wide Field-of-view Sensor (SeaWiFS) since its launch in 1997 have further refined our understanding of seasonal variation within the CCS through improved sensor characteristics and processing algorithms. The spatial and temporal averaging often applied to SeaWiFS data, however, limits the evaluation of local or mesoscale spatial pattern in seasonal dynamics [e.g., *Kahru and Mitchell*, 2001; *Thomas et al.*, 2001; *Sackmann et al.*, 2004]. Off the Baja Peninsula, however, *Espinosa-Carreon et al.* [2004] have recently described seasonal patterns of chlorophyll, SST, and sea surface height at spatial resolutions sufficient to discern variations associated with coastal topography and persistent mesoscale structure.

[9] Year-to-year variation within the CCS is forced by basin-scale changes in oceanic and atmospheric circulation, most notably associated with tropical El Niño events. Canonical El Niño conditions within the CCS include anomalous poleward transport of warm and salty (spicy) water from the south, elevated coastal sea levels, and a depressed inshore pycnocline. Upwelled water originates from above the nutricline so that near-surface nutrient concentrations and overall productivity are greatly reduced, severely affecting ecosystem structure and function [*Hickey*, 1998; *Mackas et al.*, 2006]. Reduced pigment concentrations during the El Niño of 1982–1983 constitute the strongest and most spatially extensive nonseasonal anomaly throughout the CZCS time series [*Strub et al.*, 1990; *Thomas and Strub*, 2001]. SeaWiFS time series document a dramatic reduction in the extent of elevated chlorophyll concentrations across the CCS during the 1997–1998 El Niño [e.g., *Kahru and Mitchell*, 2000; *Thomas et al.*, 2003]. In the typically oligotrophic oceanic waters offshore of southern Baja, concentrations actually increased during the El Niño winter [*Kahru and Mitchell*, 2000; *Espinosa-Carreon et al.*, 2004]. Recurrent and topographically locked circulation features provide for local mediation of interannual variations forced by El Niño or other processes. Spatial patterns of nonseasonal chlorophyll variability along the Baja coast (dominated by negative El Niño anomalies) are nearly identical to patterns of seasonal variability, suggesting a common response to variations in nutricline depth over seasonal and interannual scales mediated by local circulation [*Espinosa-Carreon et al.*, 2004].

[10] Forcing imposed from higher latitudes contributes to interannual variation across much of the CCS as well. Anomalously strong equatorward transport of cold, fresh, nutrient-rich subarctic water into the northern CCS [*Freeland et al.*, 2003; *Strub and James*, 2003] was associated with strong, positive chlorophyll anomalies across the shelves of the Pacific Northwest during much of 2001–2002 [*Thomas et al.* 2003]. Patterns of positive anomalies apparent in SeaWiFS imagery off northern California during the fall of 2002 suggest equatorward advection of hydrographic and nutrient anomalies along the California Current core [*Thomas et al.*, 2003], a process supported by hydrographic data from southern California [*Bograd and Lynn*, 2003].

3. Data and Methods

[11] The SeaWiFS mission has provided global coverage of surface chlorophyll concentrations since September 1997. Here we use Level 3 Standard Mapped Images of chlorophyll concentrations; global fields projected onto an equal-angle grid with a nominal resolution of 9 km [*Hooker and Esaias*, 1993]. Daily imagery from the fourth SeaWiFS reprocessing [*O'Reilly et al.*, 2000] spanning the period of 4 September 1997 through 5 July 2003 (2131 days) were obtained from the NASA Goddard Space Flight Center Distributed Active Archive Center and subset to the CCS study area (Figure 1). To reduce the size of the data set used in subsequent calculations, the daily 9 km data were spatially averaged according to the geometric mean of pixels lying within nonoverlapping 18 km $\times$ 18 km boxes. Time series were assembled at each grid location from log-transformed chlorophyll concentrations. Use of the geo-

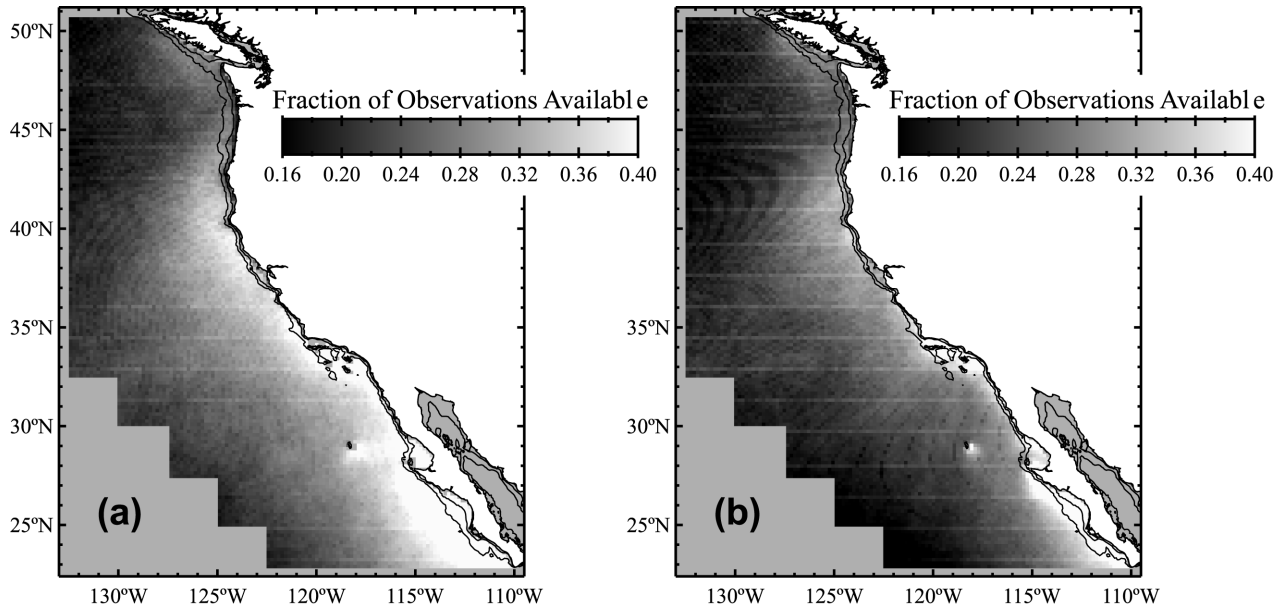

Figure 2. Number of daily observations available as a fraction of the total duration of the 2131-day time series of (a) Pathfinder SST and (b) SeaWiFS chlorophyll.

metric mean and log transformation follows the assumption that oceanic bio-optical data are distributed approximately lognormally [*Campbell*, 1995]. Chlorophyll concentrations immediately adjacent to the coastline and at specific locations (e.g., the mouth of the Columbia River and the Gulf of the Farallones (Figure 1)) may be suspect owing to the effects of colored dissolved organic matter and light-scattering inorganic particulates. Such biases are reduced by our use of 18 km box sizes and their impact on the broad-scale patterns described here is assumed to be minimal.

[12] Concurrent time series of daily sea surface temperature were assembled from the NOAA/NASA AVHRR Oceans Pathfinder equal-angle, 9 km best SST data product [*Vazquez et al.*, 1998; *Kilpatrick et al.*, 2001] provided by the NASA Physical Oceanography Distributed Active Archive Center at the Jet Propulsion Laboratory. SST estimates were derived from the Pathfinder version 4.1 (4 September 1997 to 31 December 1999) and Interim version 4.1 (1 January 2000 to 5 July 2003) algorithms using data collected from ascending passes. To reduce the size of the data set, 9 km SST data were spatially averaged according the arithmetic mean of pixels lying within nonoverlapping 18 km $\times$ 18 km boxes. Time series were then assembled at each grid location.

[13] Cloud cover and satellite orbital geometry limited the number of observations available to considerably fewer than the 2131 days spanned by the study period. Figure 2 shows the fraction of days for which SST and chlorophyll observations are available at any given location across our study region. SST estimates are typically available for about 15–55% of the total number of days. Overall patterns of chlorophyll data availability are similar to those of SST, although reduced by 5–10% in most areas. For the most part, Figure 2 reflects predominant patterns of cloud cover observed throughout the data record [*Nelson and Husby*, 1983], with reduced cloud cover closer to shore, within the SCB, and along the southern Baja coastline. Mean coastal cloud cover generally increases to the north with increasing exposure to synoptic-scale storm systems.

[14] Several patterns evident in Figure 2 appear be artifacts retained from the original 9 km global data products. Zonal bands of increased data availability are evident in both SST and chlorophyll data sets, occurring every 9 lines in the 18 km data considered here. These bands are most pronounced in the chlorophyll data (Figure 2b) where they represent an increase in data availability of $\sim$10–15%, or $\sim$200–300 additional valid retrievals compared to adjacent latitudes over the six year time series. Tests showed that this pattern is not an artifact of our own binning or plotting and that it is present in both original 9 km global data products where additional valid retrievals occur along every 18th line. This striping is apparently a computational artifact of the binning scheme used to create the 9 km global data fields and has been noticed previously (Kay Kilpatrick, RSMAS, U. Miami, personal communication, December 2004). Its presence in both the AVHRR Pathfinder and the SeaWiFS binned products results from the common heritage of the processing code [*Campbell et al.*, 1995]. A more subtle pattern composed of arcuate stripes of reduced data availability is also apparent, most clearly in the chlorophyll data (Figure 2b). This pattern likely arises through interactions between satellite orbital geometry and the remapping routines used to grid the 9 km data. Artifacts of similar appearance but at a larger spatial scale have been observed by others (G. Leptoukh, NASA GSFC, personal communication, Dec. 2004). Last, fewer SST retrievals are available for many locations immediately adjacent to the coastline (Figure 2a) owing to known deficiencies in the Pathfinder SST landmask (NOAA/NASA AVHRR Oceans Pathfinder home page, http://podaac.jpl.nasa.gov/sst/). Similarly, 18 km $\times$ 18 km averages adjacent to the coastline may be derived from fewer than four 9 km grid cells depending on the configuration of the coastline. Although present in the data and therefore incorporated into our analyses and figures,

these patterns are only marginally evident in some results at some locations and do not influence our interpretation of broad-scale spatial patterns over the CCS.

[15] Temporal variability at each grid location was divided into seasonal, interannual, and residual components. Seasonal cycles were modeled as the sum of annual and semiannual harmonics plus a constant offset (the climatological mean):

$$Z_{seas}(t) = \alpha_0 + \alpha_1 \cos(2\pi f_1 t + \zeta_1) + \alpha_2 \cos(2\pi f_2 t + \zeta_2)$$

where f_1 and f_2 are the annual and semiannual frequencies ($f_1 = 1$ cycle yr^{-1} and $f_2 = 2f_1$) and α_0, α_1, α_2, ζ_1, and ζ_2 are the offset, amplitudes, and phases estimated through ordinary least squares regression. The significance of fitted harmonic parameters was determined using a nonparametric bootstrap technique described by *Efron and Tibshirani* [1998] and similarly applied by *Michaelsen et al.* [1988]. We describe spatial patterns in seasonal cycles of SST and chlorophyll by presenting offsets, amplitudes, and phases at grid locations where estimates are significant at the 80% level. The timing of actual seasonal maxima and minima result from the combined contributions of annual and semiannual harmonics and can vary greatly between nearby locations owing to strong semiannual fluctuations. Phase estimates generally provide the clearest delineation of spatial patterns in the timing of mean seasonality.

[16] Interannual variation was calculated by applying a Gaussian kernel with a 365 day full width at half maximum to the daily time series after removal of seasonal variability. The variance of the smoothed series resulting from this step provides a relative measure of the magnitude of variability acting over interannual timescales at each grid location [e.g., *Walker and Wilkin*, 1998]. Our study period began during the El Niño of 1997–1998 just as nearshore SST anomalies across much of the northern CCS were approaching their peak. Off central Oregon in particular, a strong southwesterly storm initiated intense downwelling in late August 1997 [*Peterson et al.*, 2002], coincident with the arrival of a poleward propagating coastal wave [*Kosro*, 2002]. Equatorward currents quickly reversed and surface temperatures rose to record levels in September [*Smith et al.*, 2001; *Kosro*, 2002]. These very strong anomalies present at the beginning of our time series greatly inflated estimates of interannual SST variance along southern Oregon and northern California, producing an unduly biased depiction of patterns of interannual variability across the northern CCS. A similar bias is not apparent in patterns of chlorophyll variability, largely because the strongest nutrient and chlorophyll anomalies forced by El Niño did not occur until early or mid 1998 [e.g., *Bograd and Lynn*, 2001; *Chavez et al.*, 2002; *Espinosa-Carreon et al.*, 2004]. To obtain a less biased representation of patterns of interannual SST variance, smoothed time series were calculated over an extended period beginning on 1 April 1997. For direct comparison to SeaWiFS data, all results presented here, including maps of interannual SST variance, pertain to the period of 4 September 1997 through 5 July 2003.

[17] Following the removal of mean seasonality and interannual variation, residual time series include biological or physical variability generally acting over intraseasonal timescales, observation error, and any seasonal-scale variation not captured by stationary annual and semiannual harmonics. We present analyses of these residual time series in a companion paper (K. R. Legaard and A. C. Thomas, manuscript in preparation, 2006). Here we present spatial patterns of the percent contribution of mean seasonal cycles and interannual variability to total variance, where total variance is approximated as the sum of variance contributed by mean seasonality, interannual variability, and the dominant mode of residual intraseasonal variability. Maps of interannual variance and percent contribution to total variance have been smoothed with a 5×5 moving average to reduce speckling and emphasize large-scale patterns of interest.

[18] Eight grid locations (Figure 1) were selected to illustrate actual time series. Locations were chosen to reflect the range of seasonal, interannual, and intraseasonal behavior evident in the regional SST and chlorophyll data. Two of these locations coincide with NOAA National Data Buoy Center stations off the California coast, allowing comparisons between satellite-derived and in situ SST time series. Over the seasonal and interannual timescales presented in this manuscript, fluctuations of satellite-derived and in situ SST at these (and other) NDBC buoy locations are very similar, and comparisons are not discussed. *Dorman and Winant* [1995] describe seasonal climatologies of SST obtained from NDBC buoy data collected between 1981 and 1990.

[19] For each of the eight sample locations, a bootstrap technique was used to derive the 95% confidence levels for interannual deviations from the climatological mean. The 95% confidence level at each location is minimal through the interior of each time series and swells to a maximum over the ~4 months at the beginning and end. This swelling results from the reflection of the first and last ~8 months about the endpoints to calculate interannual variation throughout the entire study period. We report both the confidence interval valid for the interior and the confidence interval valid for the beginning and end of each time series to allow judgment of the significance of interannual variations.

4. Results and Discussion

4.1. Mean Seasonal Cycles of SST

[20] Time series at eight grid locations (Figure 1) illustrate the range of behavior of SST variability observed throughout the region (Figure 3). Mean seasonal cycles composed of annual and semiannual harmonics are superimposed. These time series contrast the stronger seasonality present at high-latitude offshore locations (Figures 3b and 3d) and near the southern Baja coast (Figure 3h) with the weaker seasonality present at inshore locations off California (Figures 3c and 3e), as documented in early publications [e.g., *Sverdrup et al.*, 1942]. Seasonal maxima generally occur in late summer. Seasonal minima occur in late winter or early spring. The timing and magnitude of seasonal extremes vary from year to year at any given location. State-space models offer an effective means of isolating such nonstationary seasonality, and their use within the CCS has similarly shown that seasonal variations of hydrographic conditions vary markedly over interannual and decadal scales [*Schwing and Mendelssohn*, 1997; *Mendelssohn et*

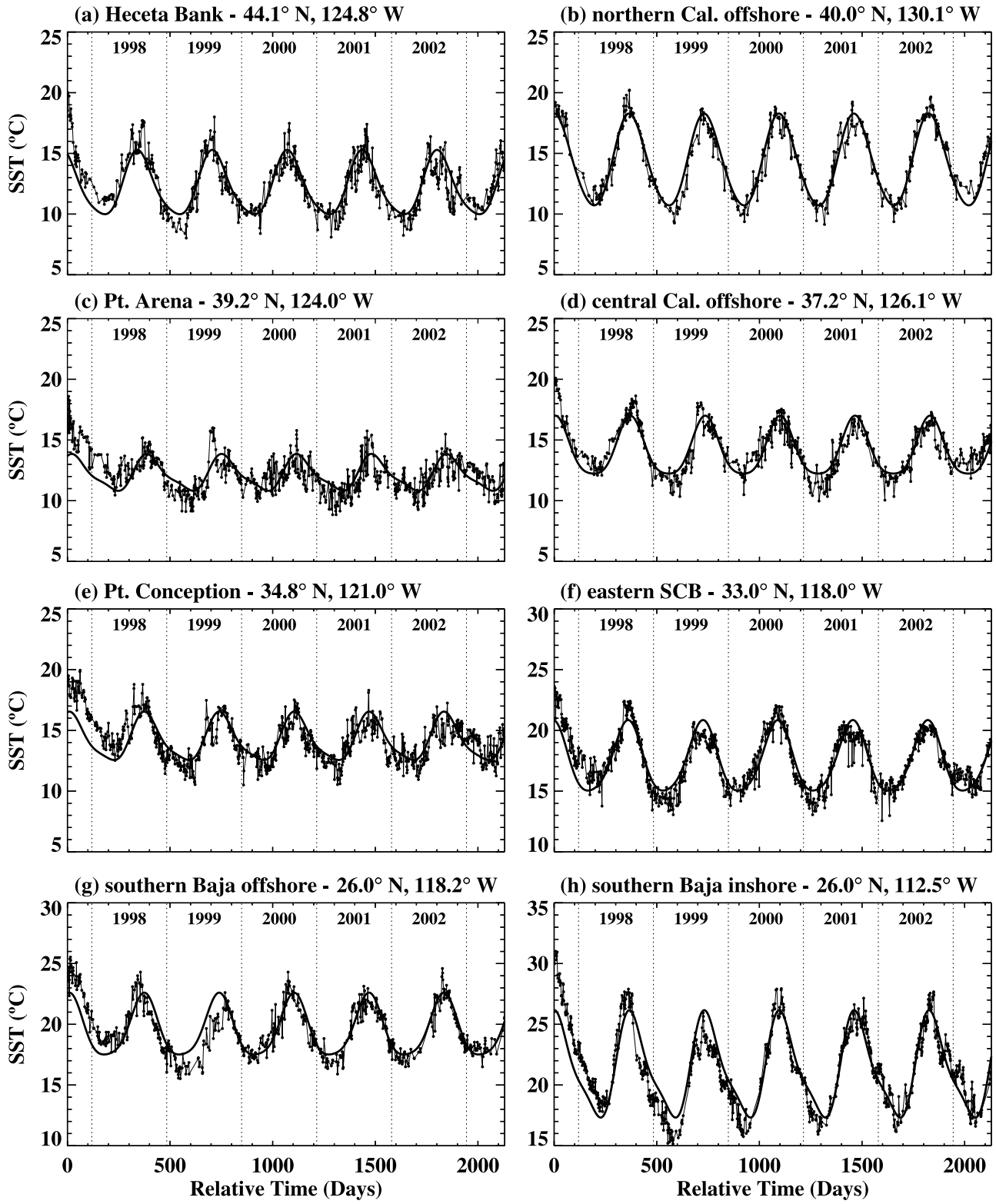

Figure 3. (a–h) SST time series assembled at the eight locations shown in Figure 1. Thick solid lines represent mean seasonal cycles estimated from annual and semiannual harmonics.

al., 2004; *Palacios et al.*, 2004]. The stationary seasonal harmonics used here provide a concise and accurate description of spatial variations in the strength and timing of mean seasonal fluctuations, against which year-to-year changes can be quantified and compared.

[21] Climatological mean surface temperatures estimated from the offset of harmonic fits (Figure 4a) show spatial patterns recognizable from any number of previous publications and are presented here for completeness. Annual amplitudes of SST (Figure 4b) are greatest seaward of the

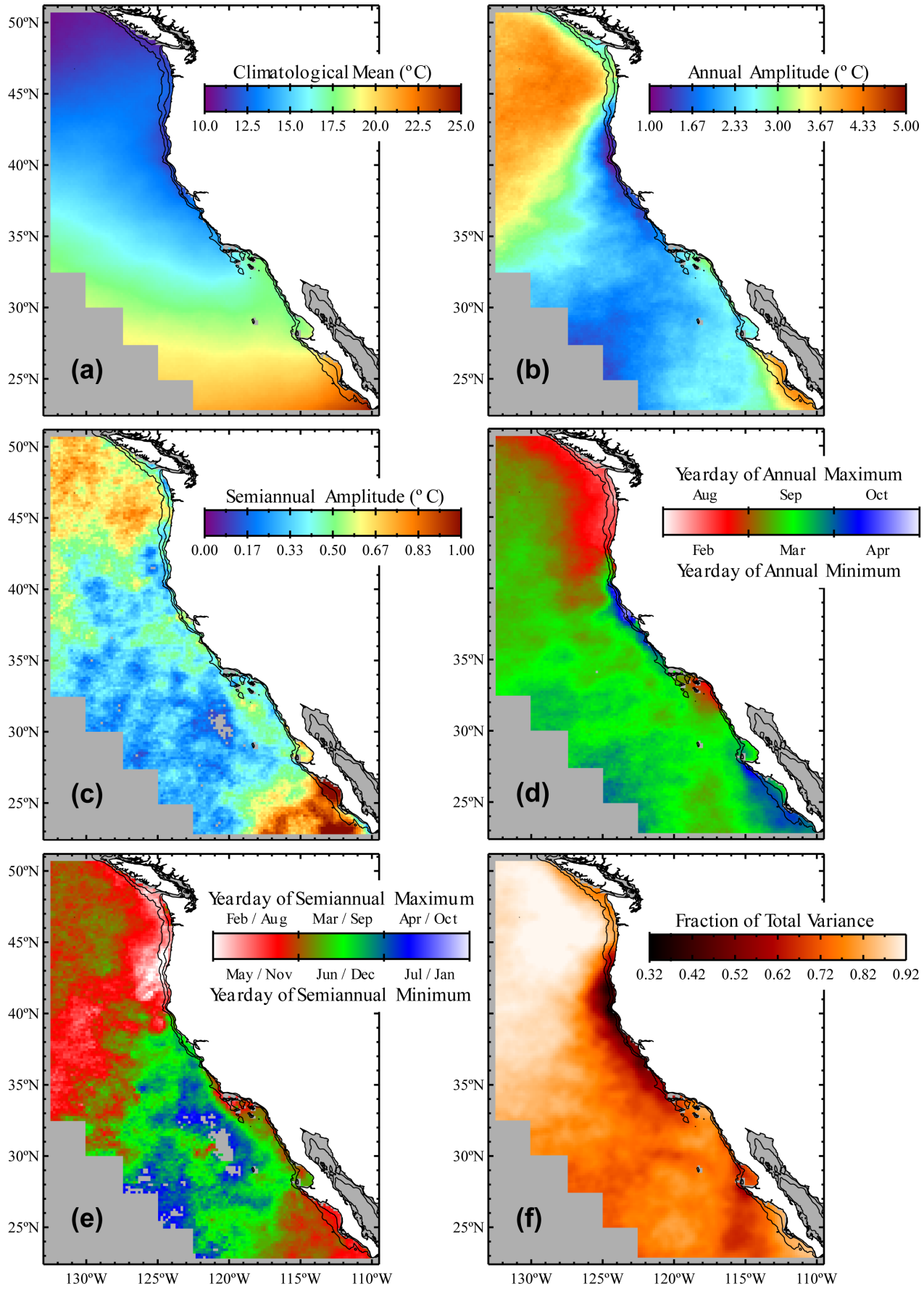
Climatological Mean (°C)
10.0 12.5 15.0 17.5 20.0 22.5 25.0
(a)
Annual Amplitude (° C)
1.00 1.67 2.33 3.00 3.67 4.33 5.00
(b)
Semiannual Amplitude (° C)
0.00 0.17 0.33 0.50 0.67 0.83 1.00
(c)
Yearday of Annual Maximum
Aug Sep Oct
Feb Mar Apr
Yearday of Annual Minimum
(d)
Yearday of Semiannual Maximum
Feb / Aug Mar / Sep Apr / Oct
May / Nov Jun / Dec Jul / Jan
Yearday of Semiannual Minimum
(e)
Fraction of Total Variance
0.32 0.42 0.52 0.62 0.72 0.82 0.92
(f)
50°N
45°N
40°N
35°N
30°N
25°N
130°W 125°W 120°W 115°W 110°W

Figure 4

continental shelf in the northwest portion of the study region and along the southern Baja shelf and slope. Upwelling north of Point Conception depresses seasonal fluctuations of nearshore SST by arresting the summer heating cycle. Minimum amplitudes are found adjacent to the coastline along southern Oregon and northern California (~39–43°N). Nearshore areas of reduced amplitude are confined to the shelf and slope north of ~45°N but expand seaward south of this latitude, consistent with the offshore expansion of upwelled waters associated with mesoscale jet and eddy activity [*Strub et al.*, 1991; *Strub and James*, 2000]. The initial seaward expansion of low amplitudes at ~45°N coincides with the broadening of the otherwise narrow and uniform Oregon shelf at Heceta Bank (Figure 1). The summertime front and jet bounding the inshore area of cool, upwelled water turn abruptly seaward at the north end of Heceta Bank and then curve cyclonically back toward shore as they round the Bank [*Barth et al.*, 2005]. The further expansion and reduction of annual amplitudes near Cape Blanco (Figure 4b) coincides with the seaward displacement of the upwelling front and jet, and the subsequent extension of a cold-water filament southwest of the Cape [*Barth et al.*, 2000, 2005].

[22] Close to the coast, consistently reduced summer cloud cover causes a strong cross-shelf gradient of incident solar radiation, increasing toward the coastline [*Nelson and Husby*, 1983]. North of Point Conception, coastal upwelling overwhelms any shoreward increase in surface heating so that annual amplitudes inshore remain lower than those offshore (Figure 4b). In the eastern SCB and along the Baja Peninsula, summer surface heating appears to play a more dominant role, and inshore SST has a stronger seasonality than offshore SST. Low amplitudes in offshore subtropical waters to the southwest are part of a swath of low seasonality extending toward the tropics beneath the southeastern flank of the North Pacific high [*Yashayaev and Zveryaev*, 2001], where extensive and persistent summer cloud cover likely curbs surface heating. High amplitudes over the shelf and slope south of Punta Eugenia (27.7°N) (Figure 1) are part of larger area of strong seasonality extending throughout much of the Gulf of California and as far south as ~20°N [*Yashayaev and Zveryaev*, 2001]. Although *Espinosa-Carreon et al.* [2004] attribute strong SST seasonality south of Punta Eugenia to upwelling and lateral heat advection, the large spatial extent of this high-amplitude area suggests that seasonal cycles of SST are more closely associated with surface heat exchange driven by the advection of continental air from the Mexican mainland [*Yashayaev and Zveryaev*, 2001].

[23] Semiannual amplitudes of SST (Figure 4c) are everywhere much less than annual amplitudes, but remain significant at most grid locations, strongest off southern Baja and across the northern portion of our study region (>44°N). Semiannual harmonics accommodate asymmetric seasonal cycles of SST by adjusting the timing of seasonal maxima and minima. We therefore interpret semiannual cycles in light of their apparent impact on the timing of mean seasonality, as indicated by annual and semiannual phase estimates.

[24] Figures 4d and 4e present the spatial patterns of annual and semiannual phases according to the yeardays of maximum and minimum SST attributable to annual and semiannual harmonics. Along the California coast between Point Conception and Cape Mendocino (40.4°N) (Figure 1), inshore annual maxima (minima) occur between late September (late March) and early October (early April), lagging those further offshore by ~2–6 weeks (Figure 4d). Semiannual harmonics with maxima (minima) in late March/September (late June/December) tend to further delay (and broaden) inshore seasonal minima (e.g., Figures 3c and 3e). Upwelling delays the arrival of seasonal maxima and minima, with the greatest delay occurring south of the upwelling center at Point Arena (39.2°N) (Figure 1). Shortly after offshore surface temperatures drop to their seasonal lows in late winter, upwelling-favorable winds begin to strengthen along the California coastline [*Dorman and Winant*, 1995]. At the onset of the spring transition, cool subsurface water floods the shelf and upper slope and inshore surface temperatures continue to cool through early and mid spring as winds strengthen toward their late spring or early summer maxima. Surface temperatures climb to their seasonal maxima in late summer or early fall once upwelling winds have weakened [*Dorman and Winant*, 1995].

[25] Nearshore annual phase estimates (Figure 4d) show a progressive shift to earlier dates from northern California into the Pacific Northwest, reflecting a shift in seasonal maxima from mid October immediately south of Point Arena to early or mid August north of Cape Blanco and a similar shift in seasonal minima from late May to early or mid February (compare Figures 3a and 3c). The shift toward winter minima north of Cape Mendocino is driven by stronger winter cooling, weaker spring upwelling, and an often delayed onset of the spring transition relative to more southerly latitudes [*Strub et al.*, 1987; *Largier et al.*, 1993; *Strub and James*, 2000]. Between Point Conception and Cape Mendocino, seasonal cycles fluctuate between spring, upwelling-driven minima and late summer maxima. North of Cape Blanco, seasonal cycles fluctuate between winter minima and summer maxima. The timing of these mean seasonal cycles agrees well with in situ time series described by *Dorman and Winant* [1995].

[26] Broad bands of August annual maxima (Figure 4d) and February/August semiannual maxima (Figure 4e) are apparent off the Pacific Northwest. August annual maxima extend northward along British Columbia and Alaska [*Yashayaev and Zveryaev*, 2001]. These areas lie within a region of excess precipitation over evaporation [*Husby and*

Figure 4. (a) Climatological mean SST estimated from the offset of the harmonic fit. Amplitude of the (b) annual and (c) semiannual harmonic. Phase of the (d) annual and (e) semiannual harmonic. (f) Fraction of total SST variance contributed by annual and semiannual harmonics. Total variance is approximated as the sum of variance contributed by the mean seasonal cycle, interannual variability, and dominant intraseasonal variability (described in a companion paper (K. R. Legaard and A. C. Thomas, manuscript in preparation, 2006)). Data in Figure 4d were smoothed with a 5 × 5 moving average.

Nelson, 1982] and beneath a band of wintertime negative wind stress curl caused by the anticyclonic turn of prevailing winds around the Aleutian low [*Murphree et al.*, 2003a]. By increasing near-surface stability, weaker summer upwelling, increased stratification, and a tendency for convergent surface flow beneath anticyclonic winter winds likely shift annual maxima and minima to earlier dates, nearer to the maxima and minima of the solar heating cycle. Freshwater discharge from the Columbia River (46.1°N) and Juan de Fuca Strait (48.2°N) (Figure 1) further increases water column stability in nearshore waters of the Pacific Northwest, likely shifting seasonal maxima and minima to still earlier dates as indicated by early August semiannual maxima (Figure 4e).

[27] Annual SST cycles off the Baja Peninsula south of Punta Eugenia show timing similar to those along central California (Figure 4d). Strong semiannual cycles peaking in late February/August (Figures 4c and 4e) shift inshore seasonal maxima along south-central Baja to mid September, nearer to seasonal maxima farther offshore (compare Figures 3g and 3h). Semiannual cycles further shift seasonal minima to late April or early May (e.g., Figure 3h) across a large area extending from the coast at Punta Eugenia to more than 500 km offshore of the southern tip of the peninsula. Although these spring seasonal minima are generally concurrent with a spring maximum in equatorward wind stress and coastal upwelling [*Thomas and Strub*, 2001; *Espinosa-Carreon et al.*, 2004], their spatial extent suggests an association with processes acting over much larger scales, such as surface cooling mediated by the advection of continental air [*Yashayaev and Zveryaev*, 2001].

[28] In the eastern SCB, annual cycles of SST (Figure 4d) with August maxima (February minima) lead the September maxima (March minima) found nearshore to the south and north and offshore to the west. Semiannual harmonics (Figure 4e) enhance the east-west contrast in the timing of seasonal minima by shifting eastern minima toward winter dates and western minima toward spring dates. Along the outer boundary of the SCB, early spring minima and late summer maxima are consistent with the southward advection of cool upwelled water from the north [*Strub and James*, 2000]. In the eastern SCB, winter minima and mid summer maxima are consistent with patterns of local wind forcing. The sharp change in coastal orientation at Point Conception shelters surface waters along the northern and eastern margins of the SCB from prevailing northwesterly winds during all seasons [*Winant and Dorman*, 1997]. Within the eastern interior of the SCB, upwelling at the onset of the spring transition is generally too weak to shift seasonal minima from the winter minima typical of oceanic waters, and reduced wind mixing throughout the spring and summer allows for a more strongly stratified upper water column [*Caldeira and Marchesiello*, 2002].

[29] Figure 4f shows the spatial pattern of the contribution of the mean seasonal cycle to total SST variance. Seasonal fluctuations account for more than 90% of total SST variance in offshore temperate waters (north of ~35°N) where annual amplitudes are high (Figure 4b). Seasonal contributions to total variance are notably depressed within ~200 km of the coast north of Point Conception to ~45°N (Figure 4f). Nearshore contributions are most strongly depressed just south of Cape Blanco and near Cape Mendocino where annual amplitudes are weakest. As previously described, the seaward expansion of low amplitudes and reduced seasonal contributions to total variance near Heceta Bank and Cape Blanco indicate a heavy influence of coastal topography and recurrent mesoscale circulation on spatial patterns of SST seasonality. Seasonal fluctuations contribute the majority of total variance across the southern CCS.

4.2. Mean Seasonal Cycles of Chlorophyll

[30] Log-transformed chlorophyll time series assembled at eight sample locations (Figure 1), with annual and semiannual harmonics superimposed, illustrate patterns of seasonal variability evident across the CCS (Figure 5). In general, seasonality is strongest at inshore locations, especially off southern Baja (Figure 5h). Seasonality is generally weak at offshore locations (e.g., Figures 5d and 5g), although not at 40°N (Figure 5b). The timing of mean seasonal cycles varies greatly between locations, with seasonal maxima occurring early (e.g., Figure 5b) as well as late (e.g., Figure 5a). Compared to SST time series from the same locations (Figure 3), the semiannual harmonic typically plays a more prominent role in describing the mean seasonality of chlorophyll. Year-to-year changes in the magnitude, timing, and duration of seasonal-scale fluctuations are generally more prominent with chlorophyll than with SST, and intense intraseasonal variability further obscures regular seasonal variation. Nevertheless, annual and semiannual harmonics capture significant and meaningful components of seasonal variability and provide a coherent synthesis of spatial patterns of mean seasonality.

[31] Climatological mean chlorophyll concentrations (Figure 6a) show patterns similar to those described by many previous publications [e.g., *Strub et al.*, 1990; *Thomas et al.*, 1994] and are shown here for completeness. Annual and semiannual amplitudes (Figures 6b and 6c) are strongest nearshore. Both are maximum over the Pacific Northwest shelf (north of Cape Blanco), driven by strong cycles of coastal wind forcing and incident solar radiation (reinforced by seasonal cycles of cloud cover). Strong annual and semiannual fluctuations extend farthest from shore off Washington and Vancouver Island. Annual amplitudes are of comparable strength along the Baja shelf south of ~30°N, but maximum amplitudes are more closely confined to the coast. A localized area of peak seasonality lies along central California near the Gulf of the Farallones and Monterey Bay (~36–38°N) (Figure 1) with considerably weaker seasonality to the immediate north and south. Weak amplitudes near Cape Mendocino and Point Arena coincide with weak seasonal cycles of SST (Figures 4b–4d) and with strong seasonal cycles of alongshore wind stress [*Dorman and Winant*, 1995; *Thomas et al.*, 2001]. Elevated amplitudes along the outer boundary of the SCB suggest strong seasonal modulation of high-pigment water extending southeast of Point Conception, as described by *Thomas and Strub* [1990]. Annual and semiannual amplitudes are weak in the eastern SCB, consistent with weak upwelling, strong summer stratification, and an inshore intrusion of oligotrophic oceanic surface water associated with an eastward branch of the California Current [*Winant and Dorman*, 1997; *Strub and James*, 2000]. Seasonal cycles in offshore areas show a strong latitudinal dependence, from weak annual and semiannual cycles south

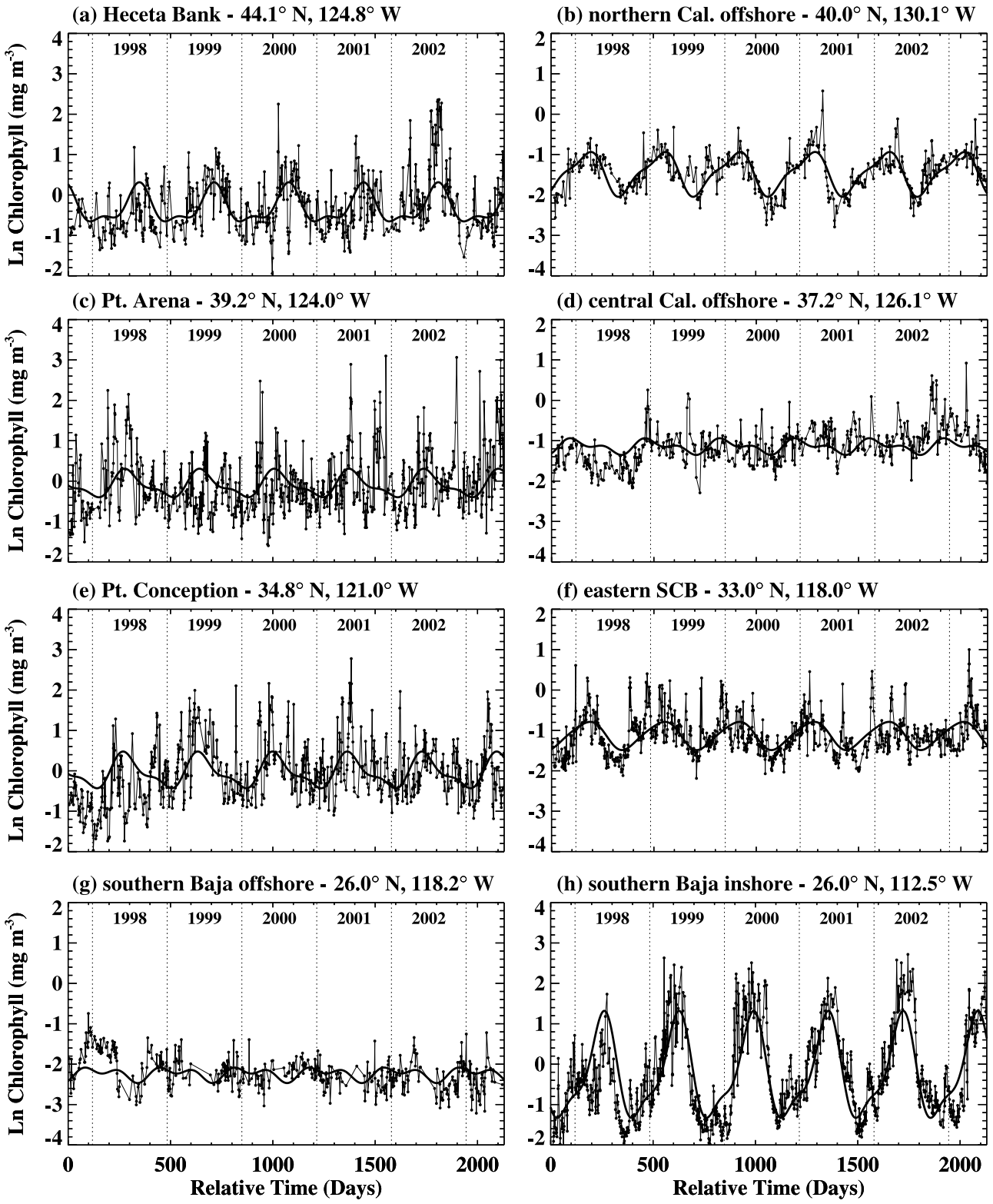

Figure 5. (a–h) Time series of log-transformed chlorophyll assembled at the eight locations shown in Figure 1. Thick solid lines represent mean seasonal cycles estimated from annual and semiannual harmonics.

of ~33°N to a dominant annual cycle between ~35°N and ~43°N, and then a weak annual and somewhat stronger semiannual cycle north of ~45°N, consistent with global patterns previously described using CZCS and SeaWiFS data [*Yoder et al.*, 1993; *Yoder and Kennelly*, 2003].

[32] Spatial patterns of annual and semiannual phase estimates (Figures 6d and 6e) are dominated by zonal

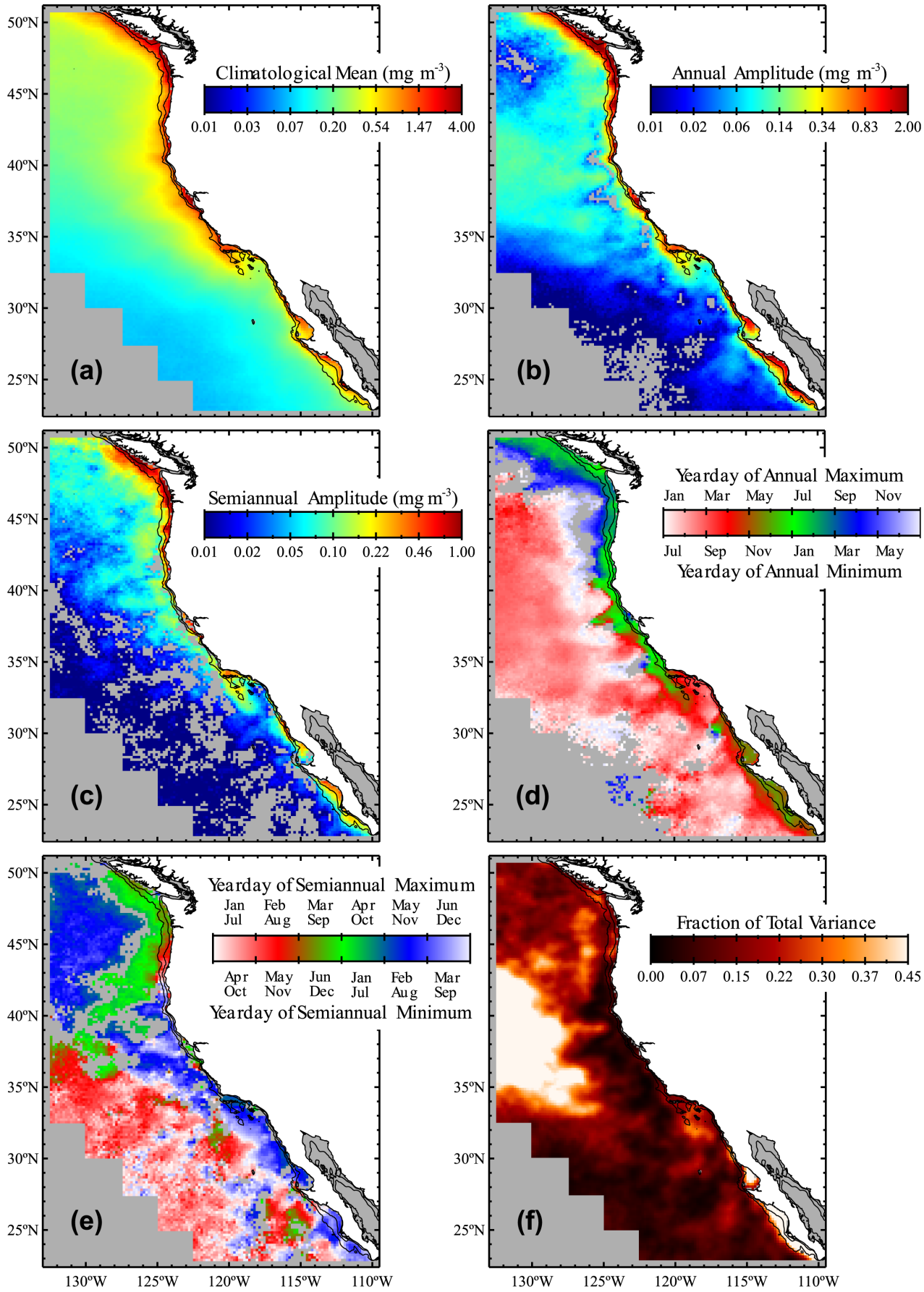
Climatological Mean (mg m-3)
0.01 0.03 0.07 0.20 0.54 1.47 4.00
(a)
Annual Amplitude (mg m-3)
0.01 0.02 0.06 0.14 0.34 0.83 2.00
(b)
Semiannual Amplitude (mg m-3)
0.01 0.02 0.05 0.10 0.22 0.46 1.00
(c)
Yearday of Annual Maximum
Jan Mar May Jul Sep Nov
Jul Sep Nov Jan Mar May
Yearday of Annual Minimum
(d)
Yearday of Semiannual Maximum
Jan Feb Mar Apr May Jun
Jul Aug Sep Oct Nov Dec
Apr May Jun Jan Feb Mar
Oct Nov Dec Jul Aug Sep
Yearday of Semiannual Minimum
(e)
Fraction of Total Variance
0.00 0.07 0.15 0.22 0.30 0.37 0.45
(f)
50°N
45°N
40°N
35°N
30°N
25°N
130°W 125°W 120°W 115°W 110°W

Figure 6

differences separating nearshore and open ocean areas. Offshore annual maxima (Figure 6d) occur in late winter, driven by a vertical flux of nutrients forced by winter wind mixing [*Chavez*, 1995; *Yoder and Kennelly*, 2003]. Nearshore annual cycles for regions north of Point Conception generally fluctuate in phase with equatorward, upwelling-favorable winds [*Thomas et al.*, 2001], resulting in summer maxima and winter minima (e.g., Figures 5a, 5c, and 5e). The scalloped boundary of summer maxima off northern and central California suggests control of summer chlorophyll distributions through recurrent patterns of mesoscale circulation. Over the south-central Baja shelf, late spring maxima lag early spring SST minima (Figure 4d) and peak equatorward wind forcing [*Thomas and Strub*, 2001; *Espinosa-Carreon et al.*, 2004]. Immediately seaward of the Baja shelf, annual chlorophyll maxima (Figure 6d) more closely coincide with peak upwelling-favorable winds. North of Cape Mendocino, annual phase estimates reflect a seaward progression from summer maxima inshore, to fall maxima immediately seaward of these, to winter maxima farther offshore, consistent with a fall expansion of high-pigment water [*Strub et al.*, 1990; *Thomas et al.*, 1994; *Thomas and Strub*, 2001]. A continuous band of insignificant annual phase estimates separates fall and winter maxima, suggesting year-to-year variability in the timing of this fall chlorophyll expansion. In temperate offshore waters north of ~40°N and within several hundred kilometers of the coast from Cape Blanco south, semiannual cycles generally peak in mid to late spring/fall (Figure 6e), consistent with the irregular occurrence of spring/fall blooms apparent in many time series (Figure 5). Late winter/summer or early spring/fall semiannual maxima lie inshore along the Pacific Northwest and extend offshore to the southwest (Figure 6e), apparently as part of a distinct band spanning the North Pacific [*Yoder and Kennelly*, 2003]. Semiannual phases shift to progressively later dates moving poleward of northern California, shifting seasonal maxima (or broadening seasonal peaks) from June–July off northern California to July August off southern Oregon and to August–September off Washington and much of Vancouver Island.

[33] Annual phase estimates emphasize the oceanic character of the eastern SCB, with winter maxima extending south along the northern Baja Peninsula, save for a small feature at 30°N, 117°W likely associated with a recurrent cyclonic eddy (Figure 6d) [*Peláez and McGowan*, 1986; *Soto-Mardones et al.*, 2004]. Weak seasonal cycles in the eastern SCB peak in mid to late winter when the thermocline is relatively deep and chlorophyll is evenly distributed throughout the mixed layer [*Michaelsen et al.*, 1988]. During spring and early summer, density layers shoal and tilt upward toward the coastline, but not so far as to allow the nutricline to intersect the surface. By early summer, biomass is concentrated within subsurface chlorophyll maxima, generally below the sampling depth of the SeaWiFS instrument [*Hayward and Venrick*, 1998; *Michaelsen et al.*, 1988]. Near-surface concentrations drop to their annual minima in mid to late summer, as surface temperatures approach their seasonal maxima (Figure 3e) and the upper water column becomes most strongly stratified [*Michaelsen et al.*, 1988].

[34] Figure 6f shows the contribution of the mean seasonal cycle to total chlorophyll variance. In offshore areas between ~35°N and ~43°N, extending inshore (east) to a scalloped boundary off California, annual cycles with winter maxima and summer minima dominate chlorophyll variability (e.g., Figure 5b). This is the eastern end of the North Pacific transition zone, a latitudinal band where summer stratification alternates with deep winter mixing and an annual "standing wave" of production migrates meridionally with the depth of the seasonal mixed layer [*Lewis et al.*, 1988]. This area lies north of subtropical oceanic areas of weak seasonality and south of subarctic oceanic areas where semiannual cycles are somewhat stronger than weak annual cycles (compare Figures 6b and 6c). Seasonal fluctuations contribute little to the total variance of nearshore chlorophyll from Cape Blanco to Point Conception, where seasonal contributions to total SST variance are also low (Figure 4f). In contrast, seasonal fluctuations contribute the majority of total chlorophyll variance over the Baja shelf south of ~30°N (Figure 6f). South of Punta Eugenia, strong chlorophyll seasonality is spatially coincident with strong SST seasonality (Figure 4b).

[35] A striking feature of the spatial pattern of chlorophyll seasonality is a narrow, meandering ribbon of weak variance lying 100–300 km offshore from Cape Blanco to central California (Figure 6f). Along northern California, this feature is defined by a ribbon of weak, statistically insignificant annual amplitude (Figure 6b) tracing the early summer path of the California Current core as it extends offshore of Cape Mendocino and Point Arena in well-defined meanders [*Kosro et al.*, 1991; *Strub et al.*, 1991; *Strub and James*, 2000]. The inshore edge of the meandering summertime jet acts as a more or less continuous physical and biological boundary. Inshore waters are cool and nutrient-rich, with variable but elevated levels of phytoplankton abundance maintained by a shallow or outcropping nutricline. Offshore surface waters are warm, stratified, and oligotrophic with low phytoplankton biomass [*Hood et al.*, 1990, 1991; *Chavez et al.*, 1991; *Kosro et al.*, 1991]. The current core separates inshore and offshore water masses whose annual cycles of near-surface chlorophyll are of comparable strength (Figure 6b) but opposing phase (Figure 6d). The path of the current core is absent from seasonal variations of SST, where inshore and offshore cycles fluctuate with more similar phases as a result of processes acting over larger spatial scales (Figure 4d).

Figure 6. (a) Climatological mean chlorophyll estimated from the offset of the harmonic fit. Amplitude of the (b) annual and (c) semiannual harmonic. Phase of the (d) annual and (e) semiannual harmonic. (f) Fraction of total chlorophyll variance contributed by annual and semiannual harmonics. Total variance is approximated as the sum of variance contributed by the mean seasonal cycle, interannual variability, and dominant intraseasonal variability (described in a companion paper (K. R. Legaard and A. C. Thomas, manuscript in preparation, 2006)). Data in Figure 6d were smoothed with a 5 × 5 moving average.

[36] The path of the California Current jet is highly variable, often stable for several weeks at a time but capable of rapid and dramatic reorientation within a matter of days [*Huyer et al.*, 1991]. The signature of a jet path within these climatological patterns of near-surface chlorophyll seasonality follows from the annual formation the jet in close association with coastal topography or shelf/slope morphology. Several numerical models have suggested the trapping of current meanders where major coastal promontories such as Cape Mendocino and Point Arena cause the seaward deflection and intensification of alongshore flow [*Haidvogel et al.*, 1991; *Batteen*, 1997; *Marchesiello et al.*, 2003]. On the basis of a series of stratified laboratory experiments, *Narimousa and Maxworthy* [1987, 1989] interpret the meander off Point Arena as the first standing wave generated by the Mendocino Ridge. The Point Arena jet lies at the northern end of a broad region of more convoluted flow along central California, where multiple filaments and jets extend from local upwelling centers and coherent equatorward flow is embedded within a rich and more varied eddy field [*Strub et al.*, 1991]. Average steric height profiles gathered along repeated cross-shelf transects off northern and central California suggest a general widening of the frontal zone south of Point Arena [*Kosro et al.*, 1991]. Consistent with chlorophyll acting as a tracer of mesoscale flow, a broad region of depressed annual amplitude and weak seasonal variation (Figures 6b and 6f) extends southward from central California and gradually blends into the very weak seasonality of the subtropical gyre. Although surface circulation seaward of the Baja shelf is generally dominated by the meandering core of the California Current [*Soto-Mardones et al.*, 2004], a coherent jet path is not apparent in climatological patterns of chlorophyll seasonality. This may follow from the extremely weak seasonality of the adjacent subtropical gyre (Figures 6b and 6c), the occurrence of inshore spring maxima at a time of less pronounced jet/eddy activity, or a generally weaker jet/eddy field as suggested by altimeter sea surface height [*Strub and James*, 2000] and drifter velocity data [*Brink et al.*, 2000]. Alternatively, *Soto-Mardones et al.* [2004] suggest that the formation and evolution of eddies and meanders off the Baja margin do not display a regular seasonal periodicity.

[37] Patterns of mean seasonality defined by annual and semiannual harmonics (Figure 6) provide a broad spatial context consistent with previously published satellite-based research [*Peláez and McGowan*, 1986; *Strub et al.*, 1990; *Abbott and Barksdale*, 1991; *Thomas and Strub*, 2001; *Thomas et al.*, 1994, 2001]. A typically diffuse bloom follows the spring transition to strong and sustained equatorward and upwelling-favorable winds. Shortly thereafter, chlorophyll-rich filaments begin to extend from local upwelling centers from southern Oregon to the Baja Peninsula. Offshore waters become increasingly stratified and nutrient depleted. The outer boundary of productive waters develops a scalloped appearance by early to mid summer as the upwelling front and jet meander offshore of the continental margin. Excluding the eastern SCB, concentrations off the coasts of California and Oregon peak at about this time, generally in phase with maximum equatorward winds and upwelling. Off northern California, the formation and evolution of the meandering current core shows sufficient seasonal regularity to be readily apparent in the climatological patterns of chlorophyll seasonality presented here. Coastal concentrations drop in mid to late summer as winds weaken and temperatures climb toward their seasonal maxima. A generally diffuse fall expansion of productive waters typically follows, as poleward coastal currents displace the summer circulation structure offshore [*Strub and James*, 2000]. Concentrations thereafter subside to winter levels.

4.3. Interannual Variability of SST

[38] Sample SST time series calculated by subtracting mean seasonal cycles from original time series are shown in Figure 7. Interannual variation is superimposed to provide an illustration of the nature of interannual fluctuations at each location. Although both the magnitude and timing of interannual fluctuations differ between locations, the interannual signal is consistently strongest at or near the start of the time series, positive through much of 1998 and then negative from late 1998 through 1999. These represent the most consistent deviations from mean seasonal cycles (Figure 3) resulting from the El Niño of 1997–1998 and the La Niña conditions that followed.

[39] Variance attributable to the interannual SST signal (Figure 8a), calculated over the period of 4 September 1997 through 5 July 2003, is greatest off Baja from ~30°N to a zonal boundary near 24°N, concentrated inshore and extending offshore to a well-defined meridional boundary near 116°W. *Espinosa-Carreon et al.* [2004] observe a similar pattern of elevated interannual variation off Baja. Interannual variance in offshore waters is otherwise very weak, save for an area of elevated variance in the northwest, between ~43°N and ~50°N (Figure 8a). Variance is moderately elevated along central California with a local maximum in the Gulf of the Farallones and Monterey Bay, along the outer boundary of the SCB, and along southern Oregon over Heceta Bank and extending offshore to the southwest of Cape Blanco. Nearshore interannual variance is weakest near the mouth of the Columbia River and in the eastern SCB. Local patches of relatively low variance lie near Cape Mendocino, Point Arena, and Point Conception.

[40] The fraction of total SST variance attributable to interannual variation is shown in Figure 8b. Interannual variability within ~100 km of the coast along southern Oregon and north-central California is a major contributor to total SST variance, in part because mean seasonal fluctuations throughout this area are very weak (Figure 4). Interannual contributions are lower off Baja, where strong interannual variation is dominated by still stronger seasonal variation.

[41] The primary contributor to patterns of interannual SST variance (Figure 8) observed during the study period is the 1997–1998 El Niño (Figure 7). Off the Baja Peninsula, anomalous advection played a dominant role in the evolution of water property anomalies during peak El Niño conditions [*Durazo and Baumgartner*, 2002]. Hydrographic data from October 1997 and January 1998 indicate that cool and fresh subarctic water within the California Current core was deflected offshore of ~116°W by an intruding mass of high-temperature, high-salinity surface water, originating in the subtropical gyre to the west and subsequently entrained within a broad system of poleward surface currents. The pattern of elevated SST variance off Baja California (Figure 8a) is similar to the January 1998 pattern of

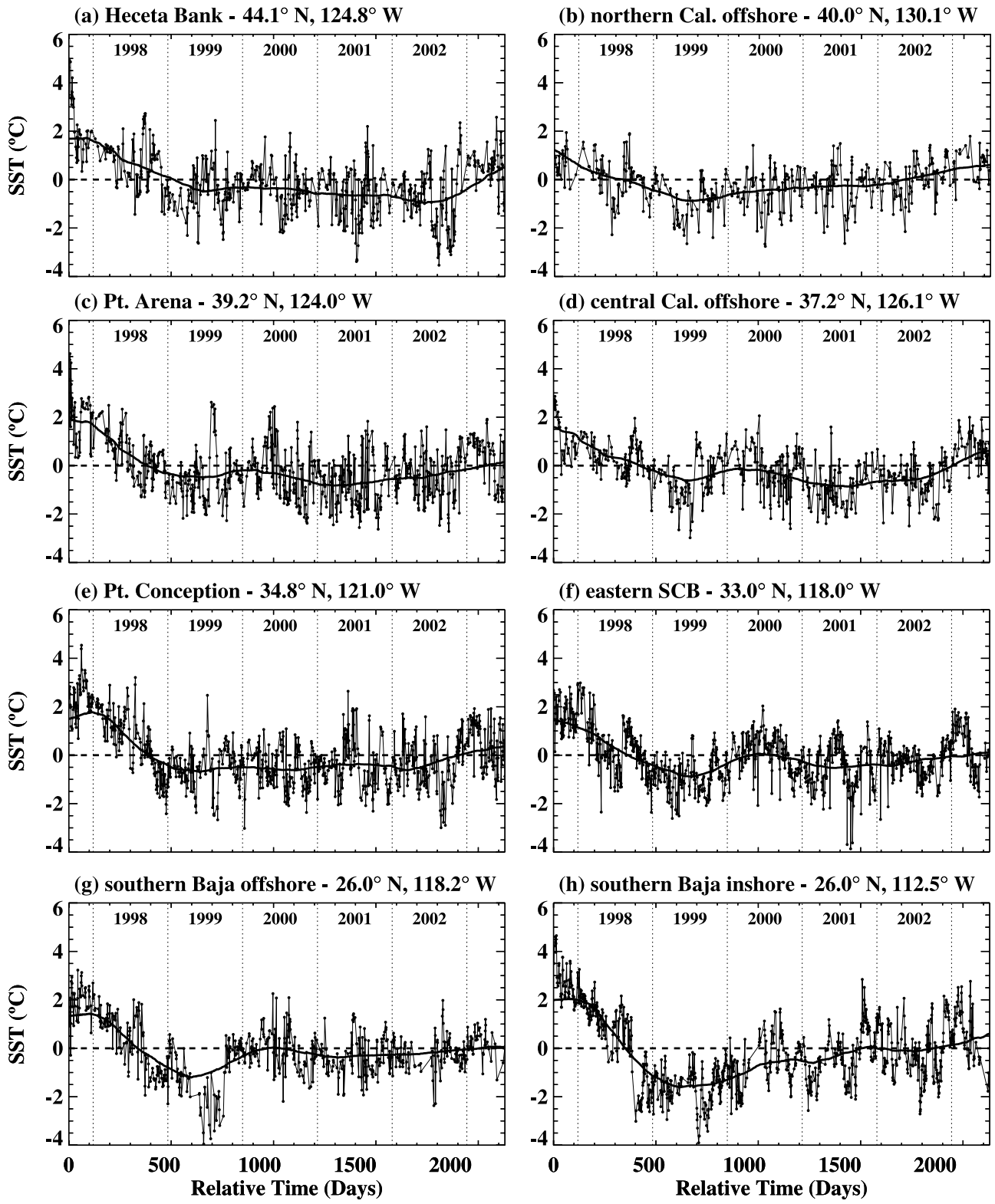

Figure 7. (a–h) SST time series calculated by subtracting mean seasonal cycles from the original time series assembled at the eight locations shown in Figure 1. Thick solid lines represent interannual variation. The 95% confidence levels for interannual variation over all eight locations are less than ±0.19°C in the interior of the time series and swell to no more than ±0.36°C at the beginning and end of the time series.

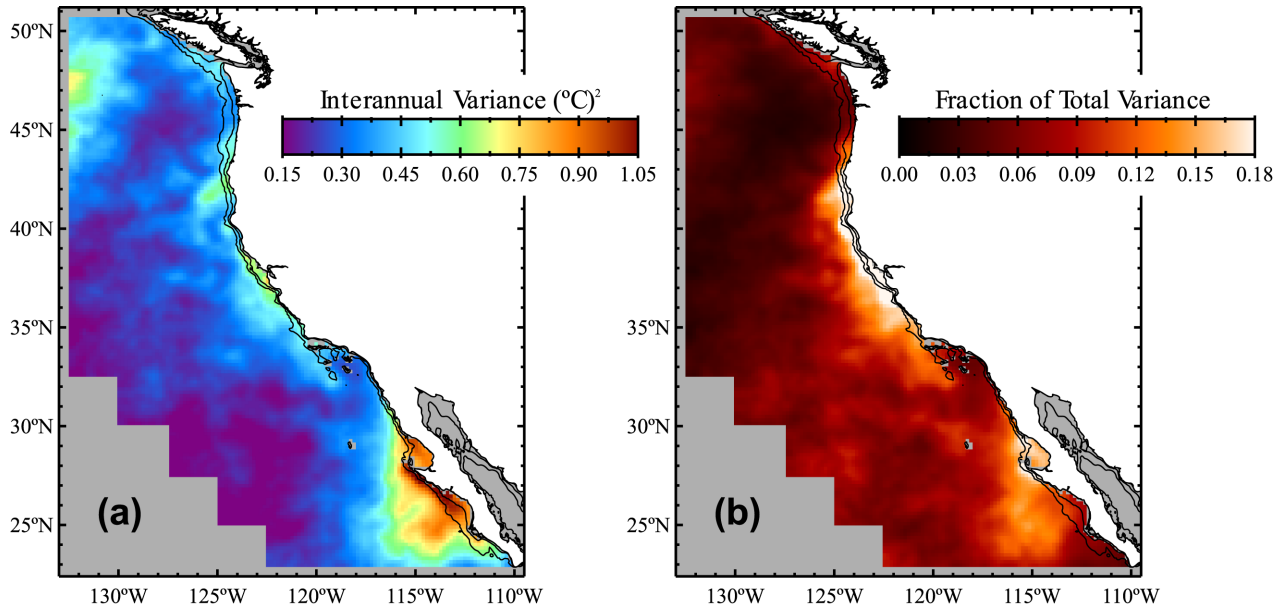

Figure 8. (a) Interannual variance of SST, estimated as the variance of smoothed time series obtained by applying a low-pass Gaussian filter following the removal of mean seasonality. (b) Fraction of total SST variance contributed by interannual variability. Total variance is approximated as the sum of variance contributed by the mean seasonal cycle, interannual variability, and dominant intraseasonal variability (described in a companion paper (K. R. Legaard and A. C. Thomas, manuscript in preparation, 2006)). Data in Figures 8a and 8b were smoothed with a 5 × 5 moving average.

elevated near-surface spiciness reported by *Durazo and Baumgartner* [2002, Figure 10b], although these authors do not resolve the outer boundary of this feature south of ~27°N. An eastward intrusion of warm subtropical water, however, may explain the sharp drop in SST variance at ~24°N (Figure 8a). Were warm El Niño anomalies off the Baja coast caused by an intrusion of tropical surface water from the south rather than subtropical surface water from the west, we could expect elevated levels of interannual SST variance to extend south of 24°N.

[42] Residual time series and monthly SST anomalies (not shown) suggest that the spatial pattern of interannual variance along Oregon and California (Figure 8) is largely a product of the relative intensity of anomalies present at or near the beginning of our study period. The summer of 1997 was one of record low upwelling off central Oregon, with surface temperatures already approaching typical seasonal maxima by early summer [*Peterson et al.*, 2002]. The passage of a southwesterly storm and poleward propagating coastal wave initiated the reversal of equatorward currents in late August, and surface temperatures rose to record levels in September [*Smith et al.*, 2001; *Kosro*, 2002; *Peterson et al.*, 2002]. Farther to the south, sustained poleward wind anomalies were not apparent until winter 1997–1998 [*Lynn et al.*, 1998]. Surface temperatures off central California peaked with the passage of a coastal wave in August but dropped thereafter [*Chavez et al.*, 2002; *Kosro*, 2002] following an episode of anomalously strong equatorward wind forcing [*Schwing et al.*, 2002]. Nearshore equatorward flow resumed through September and cool upwelling filaments were visible off central and northern California [*Strub and James*, 2002]. Weak upwelling filaments appear to have mitigated warm El Niño anomalies near several major coastal promontories off central and northern California, resulting in local patches of relatively weak interannual SST variance (Figure 8). By late September, these upwelling filaments were severely reduced in length and intensity [*Strub and James*, 2002] as surface temperature, sea surface height, and thermocline depth anomalies continued to build through late 1997 and into early 1998 [*Lynn et al.*, 1998; *Kosro*, 2002; *Schwing et al.*, 2002; *Strub and James*, 2002].

[43] Surface temperatures throughout the CCS fell to near normal levels during the spring and summer of 1998 (Figure 7) and there were clear indications of a basin-wide transition to La Niña by July [*Hayward et al.*, 1999; *Schwing et al.*, 2002; *Venrick et al.*, 2003]. Cool La Niña conditions intensified during the latter half of 1998 and lingered over the northeast Pacific for the next three years. Positive sea level pressure and anticyclonic wind anomalies forced unusually strong upwelling, low coastal sea levels and strengthened equatorward flow throughout the CCS [*Hayward et al.*, 1999; *Venrick et al.*, 2003]. Off Baja California, cool anomalies of 1999 are of similar magnitude to the preceding warm El Niño anomalies (Figures 7g and 7h). Cool La Niña anomalies are weaker across the northern CCS (Figures 7a–7e), although they generally remain significant through 2001 at inshore locations.

[44] Anomalous atmospheric conditions established with the onset of La Niña led to a massive intrusion of subarctic water into the northern CCS during the summer of 2002 [*Freeland et al.*, 2003; *Murphree et al.*, 2003b; *Strub and James*, 2003; *Venrick et al.*, 2003]. Cool temperatures and low salinities associated with this intruding mass were centered in the upper pycnocline and were responsible for spiciness anomalies on par with those of the 1997–1998

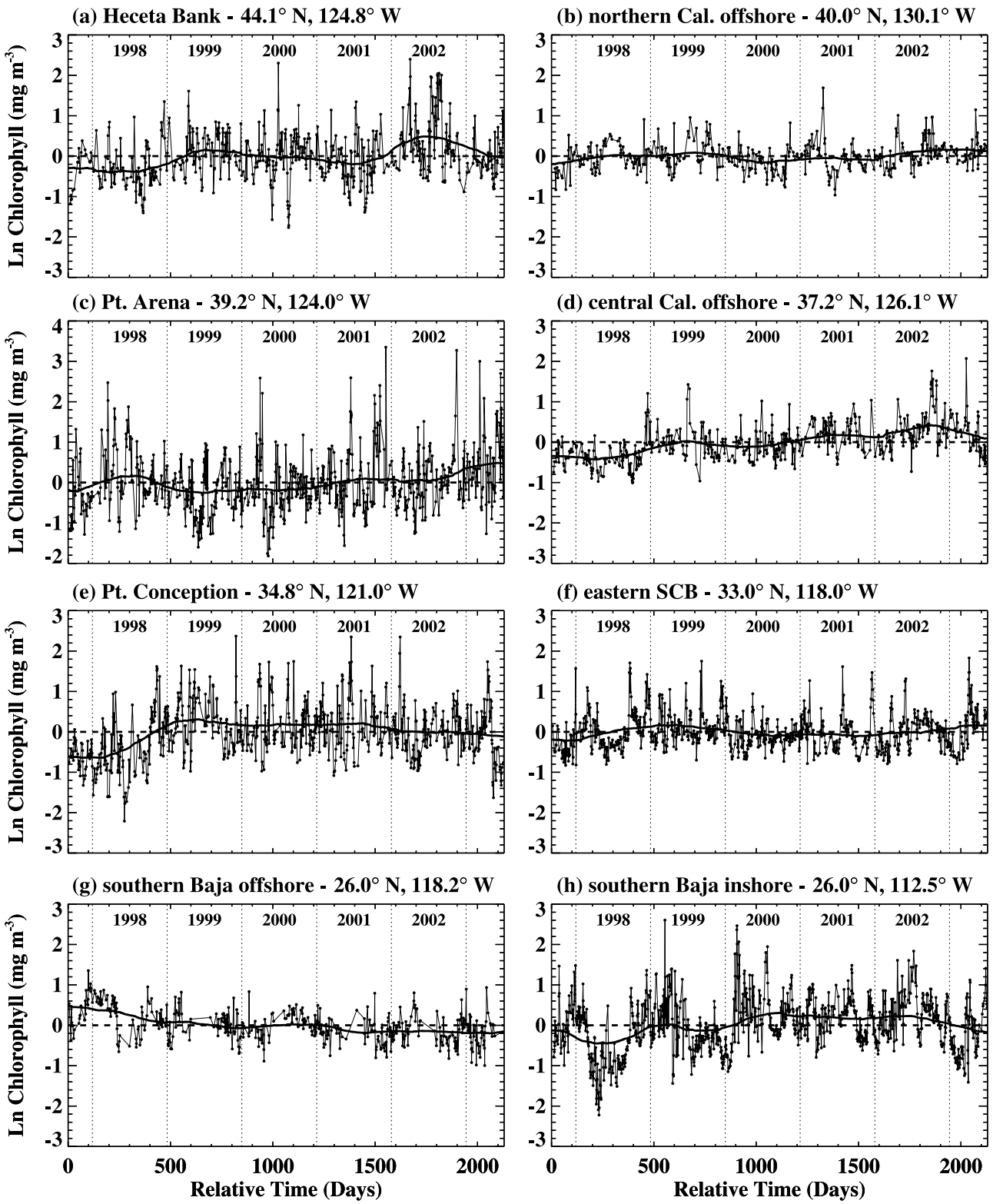

Figure 9. (a–h) Time series of log-transformed chlorophyll calculated by subtracting mean seasonal cycles from the original time series assembled at the eight locations shown in Figure 1. Thick solid lines represent interannual variation. The 95% confidence levels for interannual variation over all eight locations are less than ±0.10 log chlorophyll units in the interior of the time series and swell to no more than ±0.17 log chlorophyll units at the beginning and end of the time series.

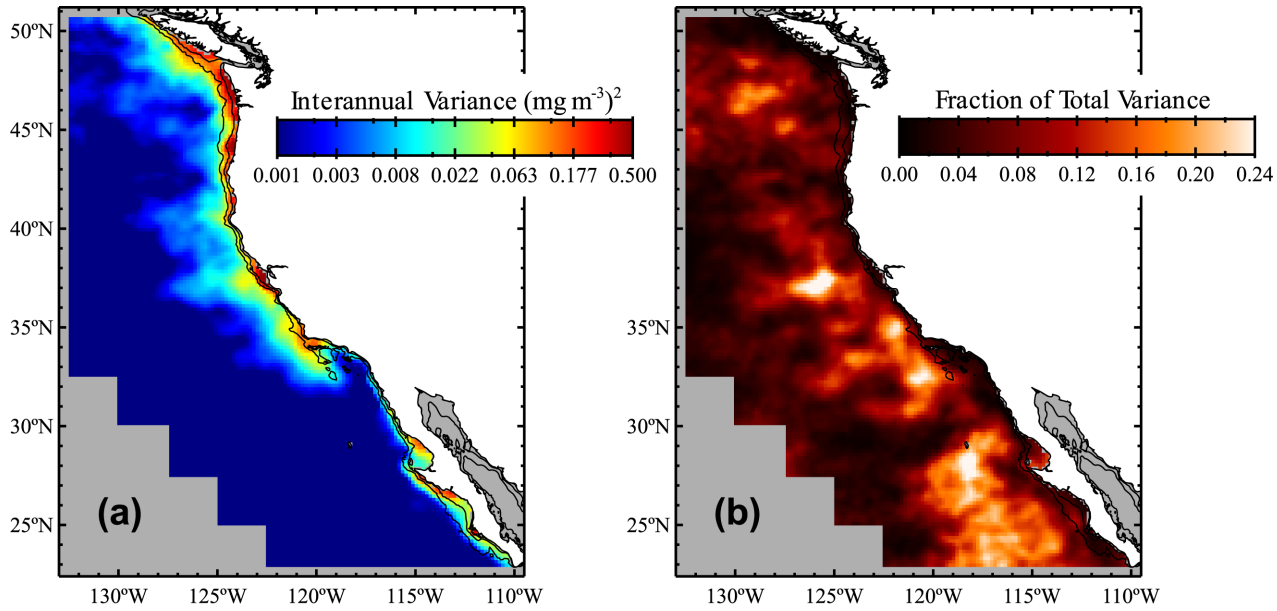

Figure 10. (a) Interannual variance of chlorophyll, estimated as the variance of smoothed time series obtained by applying a low-pass Gaussian filter following the removal of mean seasonality. (b) Fraction of total chlorophyll variance contributed by interannual variability. Total variance is approximated as the sum of variance contributed by the mean seasonal cycle, interannual variability, and dominant intraseasonal variability (described in a companion paper (K. R. Legaard and A. C. Thomas, manuscript in preparation, 2006)). Data in Figures 10a and 10b were smoothed with a 5 × 5 moving average.

El Niño (but of opposite sign), observed from Vancouver Island [*Freeland et al.*, 2003] to southern California [*Bograd and Lynn*, 2003]. These cool anomalies contribute to interannual SST variance along the shelves of the Pacific Northwest (e.g., Figure 7a) but are less apparent farther to the south (e.g., Figures 7c and 7e) and farther offshore (e.g., Figures 7b and 7d). The impact of the subarctic intrusion on surface temperatures across the northern CCS was apparently mitigated by the development of El Niño conditions during the latter half of 2002 [*Murphree et al.*, 2003b; *Venrick et al.*, 2003]. Moderate but persistent negative anomalies during the La Niña of 1999–2001 and stronger positive anomalies during the El Niño of 2002–2003 are primarily responsible for elevated interannual SST variance across temperate oceanic waters in the northwest corner of our study region.

4.4. Interannual Variability of Chlorophyll

[45] Phytoplankton abundance was reduced to well below typical levels throughout much of the CCS during the El Niño of 1997–1998 [e.g., *Kahru and Mitchell*, 2000; *Bograd and Lynn*, 2001; *Chavez et al.*, 2002; *Kudela and Chavez*, 2002; *Thomas et al.*, 2003; *Espinosa-Carreon et al.*, 2004; *Sackmann et al.*, 2004]. Off Monterey Bay, where in situ time series of nutrient and chlorophyll concentrations are relatively complete, negative surface chlorophyll anomalies began to build in early August 1997 with the intensification of coastal thermocline depth and SST anomalies [*Chavez et al.*, 2002]. The nutricline progressively deepened through the fall and winter, leading to the collapse of coastal chlorophyll and an inshore incursion of oligotrophic waters which persisted through the spring and summer of 1998. The recovery of near-surface nutrient and chlorophyll concentrations coincided with the onset of La Niña conditions in late 1998 [*Chavez et al.*, 2002].

[46] Negative El Niño anomalies observed through the first year of the SeaWiFS mission dominate interannual variability at many inshore locations (Figure 9). The response of surface chlorophyll concentrations to El Niño conditions, however, is more variable than that of SST (compare Figures 7 and 9). Off southern Baja, where positive SST anomalies are associated with reduced chlorophyll concentrations over the shelf and slope (Figure 9h), offshore concentrations actually increased during the late fall of 1997 and winter of 1997–1998 (Figure 9g), as reported by *Kahru and Mitchell* [2000]. Weak and marginally significant positive anomalies are evident off Point Arena in mid 1998 (Figure 9c). The recovery of chlorophyll to near normal levels generally coincided with the drop of surface temperatures in late 1998 (Figures 7 and 9). Positive anomalies forced by cool La Niña conditions provide substantial contributions to interannual chlorophyll variation at several inshore locations (Figure 9).

[47] Spatial patterns in the magnitude of interannual chlorophyll variability (Figure 10a) are similar to patterns of both mean concentrations (Figure 6a) and annual and semiannual amplitudes (Figures 6b and 6c), greatest over shelf and slope waters and weakest offshore. Inshore maxima are strongest in the Pacific Northwest, particularly over Heceta Bank and the Washington shelf. Localized maxima appear off central California near the Gulf of the Farallones, immediately south of Point Conception, and over the central Baja shelf. Elevated levels of interannual variance extend farthest seaward off central California and the Pacific Northwest (~400 km offshore). Inshore interannual variance is especially low above the deep basins of the

eastern SCB and along northern Baja. Similarities between patterns of interannual variance, seasonal amplitudes, and mean concentrations suggest that dominant causes of interannual variability are strong, sustained, and widespread anomalies in the vertical displacement of the nutricline during periods of seasonal upwelling or downwelling. Areas of the strongest interannual variance of SST (Figure 8a) are not identifiable as areas of particularly strong chlorophyll variance (and vice versa). Where near-surface temperature anomalies evolve somewhat independently of thermocline/nutricline depth anomalies, SST need not reflect the physical events of greatest biological importance.

[48] Within ~100 km of the coast, interannual contributions to total chlorophyll variance are weak (Figure 10b). Seasonal variation dominates total chlorophyll variance along the Baja coast south of ~30°N (Figure 6f), and residual variation dominates elsewhere. Weak inshore interannual contributions are consistent with in situ and prior satellite-derived observations. Whether maintained by episodic upwelling, mixing over the shallow shelf, runoff, or other means of enrichment, chlorophyll concentrations and modeled levels of new production near the coast at Monterey Bay were less sensitive to the El Niño conditions of 1997–1998 than those farther from the coast [*Chavez et al.*, 2002; *Kudela and Chavez*, 2002]. From five years of CZCS data, *Thomas and Strub* [2001] found that the most consistent patterns of interannual variation in cross-shelf pigment distributions occur seaward of a narrow coastal band, with regions 100–300 km offshore more susceptible to deviations during El Niño and La Niña years. Patterns of interannual contributions to total chlorophyll variance contrast strongly to those of SST, where interannual contributions are strongest nearshore (Figure 8b).

[49] Positive chlorophyll anomalies during the 1997–1998 El Niño winter are responsible for a large area of increased interannual contribution lying ~100–700 km offshore of the Baja Peninsula (Figure 10b). *Kahru and Mitchell* [2000] suggest that elevated concentrations within these oligotrophic waters may have been caused by blooms of nitrogen-fixing cyanobacteria. *Espinosa-Carreon et al.* [2004] argue that the phytoplankton assemblages responsible for these anomalies would have had to contain large concentrations of cells other than cyanobacteria to explain the high chlorophyll concentrations detected by standard SeaWiFS ocean color algorithms. The latter hypothesis suggests an unusual enrichment of offshore waters either through the upward entrainment of nutrients or through the advection of phytoplankton or nutrients from the north or east. Patterns of global chlorophyll variability presented by *Yoder and Kennelly* [2003] indicate that the positive anomalies present off Baja during early 1998 were part of a larger block of elevated chlorophyll extending across the eastern subtropical Pacific.

[50] Between ~100 and ~500 km off the California coast south of Pt. Arena, interannual contributions to total chlorophyll variance (Figure 10b) exceed seasonal contributions (Figure 6f) within several discrete mesoscale patches. The consolidation of large interannual contributions within localized patches suggests control of interannual variability through sustained variations in mesoscale circulation (e.g., variations in the path of the California Current core, the lengths and strengths of local upwelling jets and filaments, or the locations and intensities of mesoscale eddies). Concomitant changes in nutricline topography and in the cross-shelf exchange of nutrients and phytoplankton may contribute to cross-shelf chlorophyll variability over interannual scales. Strongly reduced mesoscale activity was observed offshore of the Baja Peninsula during the 1997–1998 El Niño [*Durazo and Baumgartner*, 2002]. A virtual absence of upwelling weakened frontal structure and reduced cross-shelf dynamic height gradients, weakening alongshore flow. As a result, instability processes played a lesser role in generating mesoscale structure. Energetic patterns of surface circulation dominated by an intensified California Current core returned with the transition to La Niña conditions during the latter half of 1998 [*Durazo and Baumgartner*, 2002]. Similar conditions likely occurred off California. The patches of strong interannual variance located at ~37°N, 126°W and ~32°N, 121°W (Figure 10b) lie near strong, seasonally persistent frontal features. The patch at ~37°N lies at the offshore terminus of a prominent and seasonally recurrent meander of the summertime California Current core (Figure 6) [*Strub et al.*, 1991]. The patch at ~32°N lies along the outer boundary of the seasonally recurrent Southern California Eddy [*Lynn and Simpson*, 1987; *Thomas and Strub*, 1990]. Both features are associated with strong chlorophyll gradients [e.g. *Thomas and Strub*, 1990; *Abbott and Barksdale*, 1991], suggesting that interannual variations in mesoscale circulation are a major contributor to interannual chlorophyll variability at these locations.

[51] Elevated chlorophyll concentrations during the subarctic intrusion of 2002 contribute substantially to interannual variance over the shelves of the Pacific Northwest (e.g., Figure 9a). Within the mesoscale patches of strong interannual contributions off California (Figure 10b), positive anomalies of late 2002 and early 2003 contribute to interannual variation roughly as much as the negative anomalies of the 1997–1998 El Niño (e.g., Figure 9d). Strong offshore contributions are consistent with strong positive chlorophyll anomalies observed more than 400 km offshore of northern California during the fall of 2002 [*Thomas et al.*, 2003] and with elevated near-surface nutrient and chlorophyll concentrations observed outside the SCB in July 2002 [*Bograd and Lynn*, 2003]. These observations suggest that, in addition to El Niño conditions imposed from the south, anomalous forcing at the northern boundary of the CCS is a strong source of interannual chlorophyll variability across much of the region.

5. Summary

[52] We have used concurrent six year time series of daily satellite-derived SST and chlorophyll to quantify temporal variability over seasonal and interannual scales across the CCS. Results presented here highlight spatial patterns and geographic boundaries of characteristic features of seasonal and interannual variation. We caution, however, that because our study period is relatively short, and because it began well after the onset of the 1997–1998 El Niño, our results may present a somewhat biased depiction of characteristic patterns of SST and chlorophyll variance acting over interannual scales.

[53] Strong coastal upwelling along central and northern California arrests summer heating, depresses seasonal cycles of SST within several hundred kilometers of the coast, and determines annual and semiannual phases inshore, where SST fluctuates between spring minima and late summer maxima. Inshore chlorophyll concentrations generally peak in early summer, with spatial patterns determined in part by the position of the seasonally recurrent California Current core. In offshore oceanic areas, winter SST minima coincide with winter chlorophyll maxima as surface cooling and wind mixing introduce nutrients into the upper ocean. Annual amplitudes of surface chlorophyll are depressed along the boundary between inshore summer maxima and offshore summer minima. Off northern California, this boundary coincides with the path of the current core as it meanders seaward of Cape Mendocino and Point Arena.

[54] Seasonal cycles of SST and chlorophyll differ in coastal areas farther to the north and south. Propagating storms dominate wind forcing throughout the Pacific Northwest, where summer upwelling-favorable winds are weaker, more variable, and persist over a shorter season. SST fluctuates between winter minima and summer maxima. Chlorophyll seasonality is strong, with summer maxima arriving at progressively later dates moving northward from Cape Mendocino. Seasonal cycles in the eastern SCB are more oceanic in character. Chlorophyll concentrations peak in mid to late winter when the upper ocean is well mixed and surface temperatures are low. Along the central and southern Baja coast, upwelling-favorable winds persist year-round but are generally weaker than off northern and central California. Very strong SST seasonality along the Baja shelf south of Punta Eugenia may be driven more by cycles of surface heat exchange than by upwelling, although spring minima coincide with the strongest wind forcing. Chlorophyll variability is dominated by a strong seasonal cycle peaking in late spring.

[55] Warm El Niño conditions of 1997–1998 represent the most prominent and spatially extensive contributions to interannual SST variance. Levels of interannual variance are strongest off south-central Baja and moderately elevated inshore from Point Conception to central Oregon and along the outer boundary of the SCB. Local upwelling near Cape Mendocino, Point Arena, and Point Conception appears to have mitigated El Niño anomalies to some extent. Cool La Niña conditions of 1999–2001 contributed greatly to elevated levels of interannual variance off Baja but had a lesser impact on SST across the northern CCS. Elevated levels of interannual chlorophyll variance show a similar spatial pattern to climatological mean concentrations and seasonal amplitudes. As a fraction of total variance, coastal concentrations are less sensitive to interannual variation than those farther ($\sim$100–500 km) from shore. Large interannual contributions to total chlorophyll variance are concentrated within discrete mesoscale patches off California, suggesting control of interannual chlorophyll variability through mesoscale circulation.

[56] As efforts to quantify and understand physical and biological variability over multiple timescales within complex oceanic systems such as the CCS intensify, the results presented here provide a background against which model output and ongoing or future time series can be compared. Our results provide essential spatial context to the many individual time series that are either in place or planned as part of coastal observing systems. Even in this six year synthesis, spatial patterns of seasonal and interannual variability show considerable mesoscale structure. This implies that mesoscale structure has sufficient seasonal recurrence, likely a result of topographic interaction, to be evident in short climatologies. It also implies that basin-scale forcing acting over interannual timescales imposes itself in many areas through changes in mesoscale pattern. In a companion paper (K. R. Legaard and A. C. Thomas, manuscript in preparation, 2006), we quantify, map, and compare intraseasonal components of SST and chlorophyll variability across this same study region.

[57] **Acknowledgments.** We acknowledge the NASA SeaWiFS Science Project and the GSFC DAAC for their efforts in making the SeaWiFS data available, the NOAA/NASA AVHRR Oceans Pathfinder project and the JPL PODAAC for access to the Pathfinder SST data, and the NOAA NDBC for access to buoy data. Support for this project was provided by NASA grants NAG5-6558, -6004 and -10620, and by NSF grant 0000899 to ACT. Insightful comments from two reviewers made the manuscript clearer and shorter. Contribution 296 from the U.S. GLOBEC Program.

References

Abbott, M. R., and B. Barksdale (1991), Phytoplankton pigment patterns and wind forcing off central California, *J. Geophys. Res.*, *96*, 14,649–14,667.

Armstrong, E. M. (2000), Satellite derived sea surface temperature variability off California during the upwelling season, *Remote Sens. Environ.*, *73*, 1–17.

Barth, J. A., S. D. Pierce, and R. L. Smith (2000), A separating coastal upwelling jet at Cape Blanco, Oregon, and its connection to the California Current System, *Deep Sea Res., Part II*, *47*, 783–810.

Barth, J. A., S. D. Pierce, and T. J. Cowles (2005), Mesoscale structure and its seasonal evolution in the northern California Current System, *Deep Sea Res., Part II*, *52*, 5–28.

Batteen, M. L. (1997), Wind-forced modeling studies of currents, meanders, and eddies in the California Current system, *J. Geophys. Res.*, *102*, 985–1010.

Beardsley, R. C., C. E. Dorman, C. A. Friehe, L. K. Rosenfeld, and C. D. Winant (1987), Local atmospheric forcing during the Coastal Ocean Dynamics Experiment: 1. A description of the marine boundary layer and atmospheric conditions over a northern California upwelling region, *J. Geophys. Res.*, *92*, 1467–1488.

Bograd, S. J., and R. J. Lynn (2001), Physical-biological coupling in the California Current during the 1997–99 El Niño-La Niña cycle, *Geophys. Res. Lett.*, *28*, 275–278.

Bograd, S. J., and R. J. Lynn (2003), Anomalous subarctic influence in the southern California Current during 2002, *Geophys. Res. Lett.*, *30*(15), 8020, doi:10.1029/2003GL017446.

Brink, K. H., R. C. Beardsley, J. Paduan, R. Limeburner, M. Caruso, and J. G. Sires (2000), A view of the 1993–1994 California Current based on surface drifters, floats, and remotely sensed data, *J. Geophys. Res.*, *105*, 8575–8604.

Caldeira, R. M. A., and P. Marchesiello (2002), Ocean response to wind sheltering in the Southern California Bight, *Geophys. Res. Lett.*, *29*(13), 1635, doi:10.1029/2001GL014563.

Campbell, J. W. (1995), The lognormal distribution as a model for bio-optical variability in the sea, *J. Geophys. Res.*, *100*, 13,237–13,254.

Campbell, J. W., J. M. Blaisdell, and M. Darzi (1995), Level-3 SeaWiFS data products: Spatial and temporal binning algorithms, in SeaWiFS Prelaunch Technical Report Series, edited by S. B. Hooker, E. R. Firestone, and J. G. Acker, *NASA Tech. Memo. 104566*, vol. 32.

Chavez, F. P. (1995), A comparison of ship and satellite chlorophyll from California and Peru, *J. Geophys. Res.*, *100*, 24,855–24,862.

Chavez, F. P., R. T. Barber, P. M. Kosro, A. Huyer, S. R. Ramp, T. P. Stanton, and B. R. de Mendiola (1991), Horizontal transport and distribution of nutrients in the coastal transition zone off northern California: Effects on primary production, phytoplankton biomass and species composition, *J. Geophys. Res.*, *96*, 14,833–14,848.

Chavez, F. P., J. T. Pennington, C. G. Castro, J. P. Ryan, R. P. Michisaki, B. Schlining, P. Walz, K. R. Buck, A. McFadyen, and C. A. Collins (2002), Biological and chemical consequences of the 1997–1998 El Niño in central California waters, *Prog. Oceanogr.*, *54*, 205–232.

Denman, K. L., and M. R. Abbott (1988), Time evolution of surface chlorophyll patterns from cross-spectrum analysis of satellite color images, *J. Geophys. Res.*, *93*, 6789–6798.

Denman, K. L., and M. R. Abbott (1994), Time scales of pattern evolution from cross-spectrum analysis of advanced very high resolution radiometer and coastal zone color scanner imagery, *J. Geophys. Res.*, *99*, 7433–7442.

Denman, K. L., and T. M. Powell (1984), Effects of physical processes on planktonic ecosystems in the coastal ocean, *Oceanogr. Mar. Biol. Annu. Rev.*, *22*, 125–168.

Dorman, C. E., and C. D. Winant (1995), Buoy observations of the atmosphere along the west coast of the United States, 1981–1990, *J. Geophys. Res.*, *100*, 16,029–16,044.

Durazo, R., and T. R. Baumgartner (2002), Evolution of oceanographic conditions of Baja California: 1997–1999, *Prog. Oceanogr.*, *54*, 7–31.

Edwards, K. A., D. P. Rogers, and C. E. Dorman (2002), Adjustment of the marine atmospheric boundary layer to the large-scale bend in the California coast, *J. Geophys. Res.*, *107*(C12), 3213, doi:10.1029/2001JC000807.

Efron, B., and R. J. Tibshirani (1998), *An Introduction to the Bootstrap*, CRC Press, Boca Raton, Fla.

Espinosa-Carreon, T. L., P. T. Strub, E. Beier, F. Ocampo-Torres, and G. Gaxiola-Castro (2004), Seasonal and interannual variability of satellite-derived chlorophyll pigment, surface height, and temperature off Baja California, *J. Geophys. Res.*, *109*, C03039, doi:10.1029/2003JC002105.

Freeland, H. J., G. Gatien, A. Huyer, and R. L. Smith (2003), Cold halocline in the northern California Current: An invasion of subarctic water, *Geophys. Res. Lett.*, *30*(3), 1141, doi:10.1029/2002GL016663.

Gallaudet, T. C., and J. J. Simpson (1994), An empirical orthogonal function analysis of remotely sensed sea surface temperature variability and its relation to interior oceanic processes off Baja California, *Remote Sens. Environ.*, *47*, 375–389.

Haidvogel, D. B., A. Beckman, and K. Hedstrom (1991), Dynamic simulation of filament formation ad evolution in the coastal transition zone, *J. Geophys. Res.*, *96*, 15,017–15,040.

Halliwell, G. R., and J. S. Allen (1987), The large-scale coastal wind field along the west coast of North America, 1981–1982, *J. Geophys. Res.*, *92*, 1861–1884.

Hayward, T. L., and E. L. Venrick (1998), Nearsurface pattern in the California Current: Coupling between physical and biological structure, *Deep Sea Res., Part II*, *45*, 1617–1638.

Hayward, T. L., et al. (1999), The state of the California Current, 1998–99: Transition to cool-water conditions, *CalCOFI Rep.*, *40*, 29–62.

Hickey, B. M. (1998), Coastal oceanography of western North America from the tip of Baja California to Vancouver Island, in *The Sea*, vol. 11, edited by A. R. Robinson and K. H. Brink, pp. 345–393, John Wiley, Hoboken, N. J.

Hill, A. E., B. M. Hickey, F. A. Shillington, P. T. Strub, K. H. Brink, E. D. Barton, and A. C. Thomas (1998), Eastern ocean boundaries, in *The Sea*, vol. 11, edited by A. R. Robinson and K. H. Brink, pp. 29–67, John Wiley, Hoboken, N. J.

Hood, R. R., M. R. Abbott, A. Huyer, and P. M. Kosro (1990), Surface patterns in temperature, flow, phytoplankton biomass, and species composition in the coastal transition zone off northern California, *J. Geophys. Res.*, *95*, 18,081–18,094.

Hood, R. R., M. R. Abbott, and A. Huyer (1991), Phytoplankton and photosynthetic light response in the coastal transition zone off northern California in June 1987, *J. Geophys. Res.*, *96*, 14,769–14,780.

Hooker, S. B., and W. E. Esaias (1993), An overview of the SeaWiFS project, *Eos Trans. AGU*, *74*, 241, 245–246.

Husby, D. M., and C. S. Nelson (1982), Turbulence and vertical stability in the California Current, *CalCOFI Rep.*, *23*, 113–129.

Hutchings, L., G. C. Pitcher, T. A. Probyn, and G. W. Bailey (1995), The chemical and biological consequences of coastal upwelling, in *Upwelling in the Ocean: Modern Processes and Ancient Records*, edited by C. P. Summerhayes et al., pp. 65–81, John Wiley, Hoboken. N. J.

Huyer, A., P. M. Kosro, J. Fleischbein, S. R. Ramp, T. Stanton, L. Washburn, F. P. Chavez, T. J. Cowles, S. D. Pierce, and R. L. Smith (1991), Currents and water masses of the coastal transition zone off northern California, June to August 1988, *J. Geophys. Res.*, *96*, 14,809–14,831.

Kahru, M., and B. G. Mitchell (2000), Influence of the 1997–98 El Niño on the surface chlorophyll in the California Current, *Geophys. Res. Lett.*, *27*, 2937–2940.

Kahru, M., and B. G. Mitchell (2001), Seasonal and nonseasonal variability of satellite-derived chlorophyll and colored dissolved organic matter concentration in the California Current, *J. Geophys. Res.*, *106*, 2517–2529.

Kelly, K. A. (1985), The influence of winds and topography on the sea surface temperature patterns over the northern California slope, *J. Geophys. Res.*, *90*, 11,783–11,789.

Kilpatrick, K. A., G. P. Podestá, and R. Evans (2001), Overview of the NOAA/NASA Pathfinder algorithm for sea surface temperature and associated match-up database, *J. Geophys. Res.*, *106*, 9179–9198.

Kosro, P. M. (2002), A poleward jet and equatorward undercurrent observed off Oregon and northern California, during the 1997–98 El Niño, *Prog. Oceanogr.*, *54*, 343–360.

Kosro, P. M., et al. (1991), The structure of the transition zone between coastal waters and the open ocean off Northern California, winter and spring 1987, *J. Geophys. Res.*, *96*, 14,707–14,730.

Kudela, R. M., and F. P. Chavez (2002), Multi-platform remote sensing of new production in central California during the 1997–1998 El Niño, *Prog. Oceanogr.*, *54*, 233–249.

Lagerloef, G. S. E. (1992), The Point Arena eddy: A recurring summer anticyclone in the California Current, *J. Geophys. Res.*, *97*, 12,557–12,568.

Largier, J. L., B. A. Magnell, and C. D. Winant (1993), Subtidal circulation over the northern California shelf, *J. Geophys. Res.*, *98*, 18,147–18,179.

Lewis, M. R., N. Kuring, and C. Yentsch (1988), Global patterns of ocean transparency: Implications for the new production of the open ocean, *J. Geophys. Res.*, *93*, 6847–6856.

Lynn, R. J., and J. J. Simpson (1987), The California Current System: The seasonal variability of its physical characteristics, *J. Geophys. Res.*, *92*, 12,947–12,966.

Lynn, R. J., et al. (1998), The state of the California Current 1997–1998: Transition to El Niño Conditions, *CalCOFI Rep.*, *39*, 25–50.

Lynn, R. J., S. J. Bograd, T. K. Chereskin, and A. Huyer (2003), Seasonal renewal in the California Current: The spring transition off California, *J. Geophys. Res.*, *108*(C8), 3279, doi:10.1029/2003JC001787.

Mackas, D. L., P. T. Strub, A. C. Thomas, and V. Montecino (2006), Eastern ocean boundaries pan-regional view, in *The Sea*, vol. 14, edited by A. R. Robinson and K. H. Brink, pp. 21–60, Harvard Univ. Press, Cambridge, Mass.

Marchesiello, P., J. C. McWilliams, and A. Shchepetkin (2003), Equilibrium structure and dynamics of the California Current System, *J. Phys. Oceanogr.*, *33*, 753–783.

Mendelssohn, R., F. B. Schwing, and S. J. Bograd (2004), Nonstationary seasonality of upper ocean temperature in the California Current, *J. Geophys. Res.*, *109*, C10015, doi:10.1029/2004JC002330.

Michaelsen, J., X. Zhang, and R. C. Smith (1988), Variability of pigment biomass in the California Current System as determined by satellite imagery: 2. Temporal variability, *J. Geophys. Res.*, *93*, 10,883–10,896.

Murphree, T., P. Green-Jessen, F. B. Schwing, and S. J. Bograd (2003a), The seasonal cycle of wind stress curl and its relationship to subsurface ocean temperature in the northeast Pacific, *Geophys. Res. Lett.*, *30*(9), 1469, doi:10.1029/2002GL016366.

Murphree, T., S. J. Bograd, F. B. Schwing, and B. Ford (2003b), Large scale atmosphere-ocean anomalies in the northeast Pacific during 2002, *Geophys. Res. Lett.*, *30*(15), 8026, doi:10.1029/2003GL017303.

Narimousa, S., and T. Maxworthy (1987), Coastal upwelling on a sloping bottom: Formation of plumes, jets and pinched-off cyclones, *J. Fluid Mech.*, *176*, 169–190.

Narimousa, S., and T. Maxworthy (1989), Application of a laboratory model to the interpretation of satellite and field observations of coastal upwelling, *Dyn. Atmos. Oceans*, *13*, 1–46.

Nelson, C. S., and D. M. Husby (1983), Climatology of surface heat fluxes over the California current region, *NOAA Tech. Rep. NMFS SSRF-763*, U. S. Dep. of Commer., Washington, D. C.

O'Reilly, J. E., et al. (2000), Ocean color chlorophyll *a* algorithms for SeaWiFS, OC2, and OC4: Version 4, in *SeaWiFS Postlaunch Calibration and Validation Analyses*, part 3, edited by S. B. Hooker and E. R. Firestone, *NASA Tech. Memo. 206892*, *11*, 9–23.

Palacios, D. M., S. J. Bograd, R. Mendelssohn, and F. B. Schwing (2004), Long-term and seasonal trend in stratification in the California Current, 1950–1993, *J. Geophys. Res.*, *109*, C10016, doi:10.1029/2004JC002380.

Peláez, J., and J. A. McGowan (1986), Phytoplankton pigment patterns in the California Current as determined by satellite, *Limnol. Oceanogr.*, *31*, 927–950.

Peterson, W. T., J. E. Keister, and L. R. Feinberg (2002), The effects of the 1997–99 El Niño/La Niña events on hydrography and zooplankton off the central Oregon coast, *Prog. Oceanogr.*, *54*, 381–398.

Sackmann, B., L. Mack, M. Logsdon, and M. J. Perry (2004), Seasonal and inter-annual variability of SeaWiFS-derived chlorophyll a concentrations in waters off the Washington and Vancouver Island coasts, 1998–2002, *Deep Sea Res., Part II*, *51*, 945–965.

Schwing, F. B., and R. Mendelssohn (1997), Increased coastal upwelling in the California Current System, *J. Geophys. Res.*, *102*, 3421–3438.

Schwing, F. B., T. Murphree, L. deWitt, and P. M. Green (2002), The evolution of oceanic and atmospheric anomalies in the northeast Pacific

during the El Niño and La Niña events of 1995–2001, *Prog. Oceanogr.*, *54*, 459–491.

Smith, R. C., X. Zhang, and J. Michaelsen (1988), Variability of pigment biomass in the California Current System as determined by satellite imagery: 1. Spatial variability, *J. Geophys. Res.*, *93*, 10,863–10,882.

Smith, R. L. (1995), The physical processes of coastal ocean upwelling systems, in *Upwelling in the Ocean: Modern Processes and Ancient Records*, edited by C. P. Summerhayes et al., pp. 39–64, John Wiley, Hoboken. N. J.

Smith, R. L., A. Huyer, and J. Fleischbein (2001), The coastal ocean off Oregon from 1961 to 2000: Is there evidence of climate change or only of Los Niños?, *Prog. Oceanogr.*, *49*, 63–93.

Soto-Mardones, L., A. Parés-Sierra, J. Garcia, R. Durazo, and S. Hormazabal (2004), Analysis of the mesoscale structure in the IMECOCAL region (off Baja California) from hydrographic, ADCP and altimetry data, *Deep Sea Res., Part II*, *51*, 785–798.

Strub, P. T., and C. James (1988), Atmospheric conditions during the spring and fall transitions in the coastal ocean off western United States, *J. Geophys. Res.*, *93*, 15,561–15,584.

Strub, P. T., and C. James (2000), Altimeter-derived variability of surface velocities in the California Current System: 2. Seasonal circulation and eddy statistics, *Deep Sea Res., Part II*, *47*, 831–870.

Strub, P. T., and C. James (2002), Altimeter-derived surface circulation in the large-scale NE Pacific Gyres, part 2: 1997–1998 El Niño anomalies, *Prog. Oceanogr.*, *53*, 185–214.

Strub, P. T., and C. James (2003), Altimeter estimates of anomalous transports into the northern California Current during 2000–2002, *Geophys. Res. Lett.*, *30*(15), 8025, doi:10.1029/2003GL017513.

Strub, P. T., J. S. Allen, A. Huyer, and R. L. Smith (1987), Large-scale structure of the spring transition in the coastal ocean off western North America, *J. Geophys. Res.*, *92*, 1527–1544.

Strub, P. T., C. James, A. C. Thomas, and M. R. Abbott (1990), Seasonal and nonseasonal variability of satellite-derived surface pigment concentration in the California Current, *J. Geophys. Res.*, *95*, 11,501–11,530.

Strub, P. T., P. M. Kosro, A. Huyer, and CTZ Collaborators (1991), The nature of cold filaments in the California Current system, *J. Geophys. Res.*, *96*, 14,743–14,768.

Sverdrup, H. U., M. W. Johnson, and R. H. Fleming (1942), *The Oceans, Their Physics, Chemistry and General Biology*, Prentice-Hall, Upper Saddle River, N. J.

Thomas, A. C., and P. T. Strub (1990), Seasonal and interannual variability of pigment concentrations across a California Current frontal zone, *J. Geophys. Res.*, *95*, 13,023–13,042.

Thomas, A., and P. T. Strub (2001), Cross-shelf phytoplankton pigment variability in the California Current, *Cont. Shelf Res.*, *21*, 1157–1190.

Thomas, A. C., F. Huang, P. T. Strub, and C. James (1994), Comparison of seasonal and interannual variability of phytoplankton pigment concentrations in the Peru and California Current systems, *J. Geophys. Res.*, *99*, 7355–7370.

Thomas, A. C., M.-E. Carr, and P. T. Strub (2001), Chlorophyll variability in eastern boundary currents, *Geophys. Res. Lett.*, *28*, 3421–3424.

Thomas, A. C., P. T. Strub, and P. Brickley (2003), Anomalous satellite-measured chlorophyll concentrations in the northern California Current in 2001–2002, *Geophys. Res. Lett.*, *30*(15), 8022, doi:10.1029/2003GL017409.

Vazquez, J., K. Perry, and K. Kilpatrick (1998), NOAA/NASA AVHRR oceans pathfinder sea surface temperature data set user's reference manual, version 4. 0, *Publ. 74 (D-14070),* Jet Propul. Lab., Pasadena, Calif.

Venrick, E., et al. (2003), The state of the California Current, 2002–2003: Tropical and subarctic influences vie for dominance, *CalCOFI Rep.*, *44*, 28–60.

Walker, A. E., and J. L. Wilkin (1998), Optimal averaging of NOAA/NASA Pathfinder satellite sea surface temperature data, *J. Geophys. Res.*, *103*, 12,869–12,883.

Winant, C. D., and C. E. Dorman (1997), Seasonal patterns of surface wind stress and heat flux over the Southern California Bight, *J. Geophys. Res.*, *102*, 5641–5653.

Yashayaev, I. M., and I. I. Zveryaev (2001), Climate of the seasonal cycle in the North Atlantic and the North Pacific oceans, *Int. J. Climatol.*, *21*, 401–417.

Yoder, J. A., and M. A. Kennelly (2003), Seasonal and ENSO variability in global ocean phytoplankton chlorophyll derived from 4 years of SeaWiFS measurements, *Global Biogeochem. Cycles*, *17*(4), 1112, doi:10.1029/2002GB001942.

Yoder, J. A., C. R. McClain, G. C. Feldman, and W. E. Esaias (1993), Annual cycles of phytoplankton chlorophyll concentrations in the global ocean: A satellite view, *Global Biogeochem. Cycles*, *7*, 181–193.

K. R. Legaard and A. C. Thomas, School of Marine Sciences, University of Maine, Orono, ME 04469, USA. (kasey_legaard@umit.maine.edu)